Supplementary Information

Effect of Intramolecular Energy Transfer in a Dual-Functional Molecular Dyad on the Performance of Solution-Processed TADF OLEDs

Na Yeon Kwon‡, Haeun Kwak‡, Ha Yeon Kim‡, Su Hong Park, Jin Young Park, Min Ji Kang, Chang Woo Koh, Sungnam Park*, Min Ju Cho*, and Dong Hoon Choi*

Department of Chemistry, Research Institute for Natural Sciences, Korea University, 145 Anam-ro, Seongbuk-gu, Seoul, 02841, Republic of Korea.

E-mail: spark8@korea.ac.kr, chominju@korea.ac.kr, dhchoi8803@korea.ac.kr

‡ N. Y. Kwon, H. Kwak, and H. Y. Kim have equally contributed to this work.

Table of Contents

1. General Information

1.1. Characterization and measurements

All UV-visible absorption spectra of the polymers in chloroform solutions and thin films were recorded using a UV-visible absorption spectrometer (Agilent 8453, photodiode array, λ = 190–1100 nm). The fluorescence (77 and 298 K) and phosphorescence (77 K, delay time = 1.0 ms) spectra were recorded using an F-7100 fluorescence spectrophotometer (HITACHI). Proton nuclear magnetic resonance (^{1}H NMR, 500 MHz) and carbon nuclear magnetic resonance (^{13}C NMR, 125 MHz) spectra were recorded in $CDCl_3$ using Varian Mercury spectrometers (Cambridge Isotope Laboratories, Inc.). Boron nuclear magnetic resonance (^{11}B NMR, 600 MHz) spectrum was recorded in $CDCl_3$ using DD2 600 MHz FT NMR (Agilent Technologies, Inc.). The masses of the synthesized compounds were determined by matrix-assisted laser desorption ionization time-of-flight (MALDI-TOF) mass spectrometry (MALDI-TOF/TOF™ 5800 system, AB SCIEX) at the Korea Basic Science Institute (Seoul). Elemental analysis was performed using a FlashSmart^{TM} elemental analyzer (Thermo Fisher Scientific).

1.2. Theoretical calculation

Density functional theory (DFT) and time-dependent DFT (TD-DFT) calculations were performed using the B3LYP functional and 6-31G(d) basis set implemented in the Gaussian 16 software package. The polarizable continuum model with integral equation formalism (IEFPCM) was used for solvation (toluene). Molecular orbitals were obtained from the optimized structures of the molecules in the ground state. The electronic excited-state energies (S_1 and T_n states) were obtained by calculating the Frank–Condon states from the ground state using TD-DFT. In addition, the natural transition orbitals (NTOs) of the electronic transitions were calculated to examine the electron- and hole-wave-functions and characterize the electronic transition properties.

1.3. Photophysical properties

TRPL signals of the doped films were analyzed using a kinetic model to solve the coupled differential equations for $[S_1]$ and $[T_1]$.[S1]

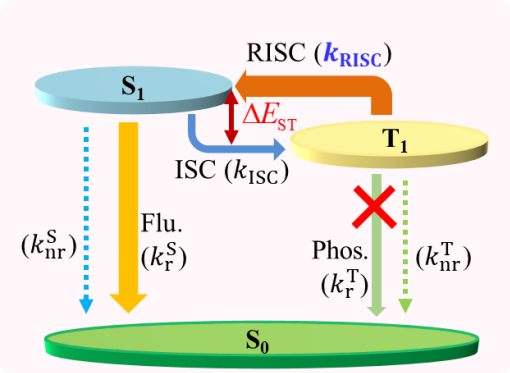

$$\frac{d[S_1]}{dt} = -(k_r^S + k_{nr}^S + k_{ISC})[S_1] + k_{RISC}[T_1]$$

$$\frac{d[T_1]}{dt} = k_{ISC}[S_1] - (k_{nr}^T + k_{RISC})[T_1]$$

Assuming that k_{nr}^T is significantly slower than k_{RISC} (i.e., $k_{RISC} \gg k_{nr}^T$), $\Phi_{\mathbf{RISC}} = k_{RISC}/(k_{nr}^T + k_{RISC}) \approx 1$. Accordingly, the rate constants associated with the TADF kinetic parameters of the doped films can be approximately determined using the following relations:

$$k_r^S = k_{PF}\Phi_{\mathbf{PF}}$$

$$k_{ISC} = k_{PF}\frac{\Phi_{\mathbf{DF}}}{\Phi_{\mathbf{PF}} + \Phi_{\mathbf{DF}}}$$

$$k_{nr}^S = k_{PF}\left(1 - \Phi_{\mathbf{PF}} - \frac{\Phi_{\mathbf{DF}}}{\Phi_{\mathbf{PF}} + \Phi_{\mathbf{DF}}}\right)$$

$$k_{RISC} = \frac{k_{PF} \cdot k_{DF}}{k_{ISC}} \cdot \frac{\Phi_{\mathbf{DF}}}{\Phi_{\mathbf{PF}}}$$

By fitting the TRPL signals (I_{PL}) with the exponential function (i.e. $I_{PL} \propto [S_1]$ and $[S_1] = A_{PF}\exp(-k_{PF}t) + A_{DF}\exp(-k_{DF}t)$), the prompt ($k_{PF} = 1/\tau_{PF}$) and delayed $k_{DF} = 1/\tau_{DF}$) fluorescence rate constants were determined. The prompt ($\Phi_{\mathbf{PF}}$) and delayed ($\Phi_{\mathbf{DF}}$) fluorescence quantum yields were determined using the area ratio of PF and DF components in the TRPL signals and the total PLQY ($\Phi_{\mathbf{PL}}$).

1.4. Angle-dependent PL intensity measurements

Angle-dependent PL measurements were performed on the doped samples prepared by solution casting on a quartz substrate. Thereafter, the film samples were placed on a fused silica half-cylinder. An index-matching gel (G608N3. Thorlabs, Inc.) was inserted between the emitting layer and half-cylinder to remove the air and match the refractive index. The film sample on the fused silica half-cylinder was excited with laser pulses generated by an Nd:YAG laser (355 nm). The p-polarized light with an incident angle of 45° was directed to the film sample. The photoluminescent emission from the sample was transmitted through a half-cylinder and collected at a series of angles using an optical fiber, mounted on a motorized rotational stage, and coupled with a monochromator and charge-coupled device (CCD). To selectively obtain only the p-polarized emissions, a polarizer was placed in front of the optical fiber. The angle was automatically controlled by a motorized rotational stage (URS100BPP, Newport Corporation) from 0° to 90°, with a resolution of 0.5°. The thickness of the doped film was 20 nm. Matlab codes were used to determine the molecular orientation in the thin films with the fitting parameter of Θ.

1.5. OLED device fabrication

OLED devices were fabricated on glass substrates coated with a transparent ITO layer (150 nm) as the anode, with a sheet resistance of 15 Ω cm^{-2} and active pattern size of 2 mm × 2 mm. The substrates were cleaned in distilled water for 10 min and isopropanol for 20 min using an ultrasonic bath, and subsequently dried using hot air. PEDOT:PSS was directly spin-coated onto an ITO plate to form a hole injection layer (30 nm) and subsequently heated at 155 °C for 15 min on a hot plate. PX2Cz dissolved in chlorobenzene was spin-coated to form a hole-transporting layer (20 nm) and subsequently heated at 130 °C for 20 min on a hot plate. A mixture of Cy-tmCP and the emitter (2-12 mol% ratio, 0.01 mol % in toluene) was spin-coated

to form an emitting layer. BmPyPB (50 nm) was used as the electron-transporting layer, and LiF (1 nm) and Al (100 nm) were vacuum-deposited in an inert chamber under a pressure of 5 × 10^{-6} Torr. The fabricated device structure consisted of ITO (150 nm), PEDOT:PSS (30 nm), PX2Cz (20 nm), Cy-tmCP emitter (20 nm), BmPyPB (50 nm), LiF (1 nm), and Al (100 nm). Fabrication was performed under ambient conditions before the substrates were placed in a thermal vacuum evaporator to evaporate BmPyPB, LiF, and Al.

2. Synthetic Procedures

2.1. Materials

All chemicals utilized in the synthesis were procured from Sigma–Aldrich and Across Organics and employed as received without additional purification. The reagent-grade solvents (e.g., toluene) utilized in this study underwent purification using standard distillation methods. Compounds **1**, **2**, **3**, and **5** were synthesized following a procedure previously reported. [S2-4]

Synthesis of Cy-CzBN (4)

Compound **2** (150 mg, 0.20 mmol), compound **3** (476 g, 0.62 mmol), and K_2CO_3 (60 mg, 0.41 mmol) were placed in a round-bottom flask with toluene-methanol-water (2:1:1) under a nitrogen atmosphere. $Pd(PPh_3)_4$ (2 mg, 0.02 mmol) was added to the solution, which was stirred at 60 °C for 12 h. After cooling to room temperature, the reaction mixture was filtered through a Celite pad. The resulting crude product was purified *via* silica gel column chromatography using CH_2Cl_2 and hexane (1:10) as the elution solvents. The purified product was filtered through methanol to obtain Cy-CzBN as a yellow powder (162 mg, 42% yield). ^{1}H NMR (500 MHz, $CDCl_3$) δ (ppm) 9.08 (d, J = 1.83 Hz, 4H), 8.51 (s, 4H), 8.42 (d, J = 1.53 Hz, 4H), 8.37 (d, J = 8.85 Hz, 4H), 8.21 - 8.26 (m, 6H), 8.13 - 8.19 (m, 4H), 7.92 (d, J = 7.93 Hz, 2H), 7.76 (t, J = 7.78 Hz, 2H), 7.57 - 7.69 (m, 10H), 7.52 (dd, J = 1.53, 8.85 Hz, 2H), 7.45 (dt, J = 1.22, 7.78 Hz, 2H), 7.28 - 7.32 (m, 2H), 2.64 (s, 4 H), 1.77 (s, 4 H), 1.65 (s, 36H), 1.61 (s, 2 H), 1.48

- 1.52 (m, 36H). ^{13}C NMR (125 MHz, CDCl3) δ ppm 145.4, 145.0, 144.8, 144.7, 143.7, 141.7, 141.0, 138.8, 138.7, 138.3, 130.6, 129.8, 127.1, 126.4, 126.2, 126.1, 125.9, 125.8, 124.6, 124.0, 123.7, 123.5, 120.7, 120.4, 120.0, 118.7, 117.3, 114.2, 109.9, 109.7, 107.0, 46.4, 38.5, 35.2, 34.8, 32.2, 31.8, 23.3. MALDI-TOF: m/z 1844.0 [M]. Elemental Anal. Calcd for $C_{134}H_{128}B_2N_6$: C, 87.27; H, 7.00; N, 4.56. Found: C, 87.07; H, 7.08; N, 4.66.

Synthesis of 9,9'-((3,3'-(cyclohexane-1,1-diyl)bis(9H-carbazole-9,3-diyl))bis(3,1-phenylene))bis(3,6-di-tert-butyl-9H-carbazole) (Cy-tmCP)

Compound **1** (433 mg, 1.04 mmol), compound **5** (1.00 g, 2.30 mmol), and *t*-BuONa (301 mg, 3.12 mmol) were placed in a round-bottom flask with dried toluene (50 mL) under a nitrogen atmosphere. $Pd_2(dba)_3$ (50 mg, 0.05 mmol) and tri-tert-butylphosphonium tetrafluoroborate (21 mg, 0.10 mmol) were added to the solution and the solution was stirred at 120 °C for 7 h. After cooling the reaction mixture to room temperature, it was filtered through a Celite pad. The resulting crude product was purified *via* silica gel column chromatography using CH_2Cl_2 and hexane (1:5) as the elution solvents. The purified product was filtered through methanol to obtain Cy-tmCP as a white solid powder (956 mg, 82% yield). ^{1}H NMR (500 MHz, $CDCl_3$) δ (ppm) 8.20 (s, 2 H), 8.12 - 8.18 (m, 6 H), 7.76 - 7.81 (m, 4 H), 7.62 - 7.67 (m, 4 H), 7.45 - 7.54 (m, 10 H), 7.39 - 7.45 (m, 6 H), 7.28 - 7.31 (m, 2 H), 2.59 (s, 4 H), 1.75 (s, 4 H), 1.60 (d, *J*=4.9 Hz, 2 H), 1.44 - 1.51 ppm (m, 36 H). ^{13}C NMR (125 MHz, CDCl3) δ ppm 143.2, 140.8, 139.7, 139.4, 138.9, 138.5, 130.9, 126.2, 125.8, 125.1, 125.1, 124.6, 123.8, 123.8, 123.5, 123.4, 120.3, 120.0, 118.5, 116.3, 109.7, 109.5, 109.1, 46.2, 38.3, 34.7, 32.0, 23.2. MALDI-TOF: m/z 1120.6 $[M]^+$. Elemental Anal. Calcd for $C_{82}H_{80}N_4$: C, 87.81; H, 7.19; N, 5.00. Found: C, 87.86; H, 7.15; N, 4.96.

Synthesis of 9-(3-(3-(1-(9H-carbazol-3-yl)cyclohexyl)-9H-carbazol-9-yl)phenyl)-3,6-di-tert-butyl-9H-carbazole (7)

Compound **1** (1.50 g, 3.61 mmol), compound **5** (1.88 g, 4.33 mmol), K_3PO_4 (1.53 g, 7.22 mmol), cuprous iodide (35 mg, 0.18 mmol), *trans*-1,2-diaminocyclohexane (0.2 ml, 0.36 mmol) and were placed in a round-bottom flask with dried toluene (50 mL) under a nitrogen atmosphere. The solution was stirred at 120 °C for 12 h. After cooling the reaction mixture to room temperature, it was filtered through a Celite pad. The resulting crude product was purified by silica gel column chromatography using CH_2Cl_2 and hexane (1:5) as the elution solvents. The purified product was filtered through methanol to obtain **7** as a solid white powder (1.88 g, 68% yield). ^{1}H NMR (500 MHz, $CDCl_3$) δ (ppm) 8.20 (s, 1 H), 8.13 - 8.18 (m, 4 H), 8.08 (d, *J*=7.63 Hz, 1 H), 7.88 (s, 1 H), 7.80 - 7.82 (m, 1 H), 7.76 - 7.80 (t, *J*=7.95 Hz, 1 H), 7.62 - 7.67 (t, *J*=7.95 Hz 2 H), 7.51 - 7.54 (m, 1 H), 7.48 - 7.51 (m, 2 H), 7.46 - 7.47 (m, 1 H), 7.39 - 7.46 (m, 4 H), 7.36 - 7.38 (m, 2 H), 7.28 - 7.31 (m, 2 H), 7.21 (m, 1 H), 2.58 (s, 4 H), 1.74 (s, 4 H), 1.61 (s, 2 H), 1.47 - 1.51 (m, 18 H). ^{13}C NMR (125 MHz, $CDCl_3$) δ ppm 143.2, 141.7, 140.8, 140.6, 139.9, 139.7, 139.4, 139.0, 138.5, 137.4, 130.9, 126.3, 126.1, 125.8, 125.5, 125.2, 125.1, 124.7, 123.9, 123.8, 123.6, 123.6, 123.4, 123.2, 120.3, 120.2, 120.0, 119.2, 118.5, 118.3, 116.3, 110.5, 110.3, 109.7, 109.5, 109.1, 70.3, 46.2, 38.3, 34.7, 32.0, 31.6, 26.6, 23.2.

Synthesis of 9-(3-(3-(1-(9-(3-bromophenyl)-9H-carbazol-3-yl)cyclohexyl)-9H-carbazol-9-yl)phenyl)-3,6-di-tert-butyl-9H-carbazole (8)

Compound **7** (400 mg, 0.52 mmol), 3-bromoiodobenzene (221 mg, 0.78 mmol), K_3PO_4 (220 mg, 1.04 mmol), cuprous iodide (5.00 mg, 0.02 mmol), *trans*-1,2-diaminocyclohexane (0.1 ml, 0.04 mmol) and were placed in a round-bottomed flask with dried toluene (30 mL) under a nitrogen atmosphere. The solution was stirred at 120 °C for 12 h. After cooling to room

temperature, the reaction mixture was filtered through a Celite pad. The resulting crude product was purified *via* silica gel column chromatography using CH_2Cl_2 and hexane (1:5) as the elution solvents. The purified product was filtered through methanol to obtain **8** as a white powder (335 mg, 70% yield). ^{1}H NMR (500 MHz, $CDCl_3$) δ (ppm) 8.17 - 8.19 (d, *J*=0.90 Hz 2 H), 8.11 - 8.15 (m, 4 H), 7.77 - 7.81 (m, 2 H), 7.71 (t, *J*=1.98 Hz, 2 H), 7.62 - 7.66 (m, 2 H), 7.54 - 7.57 (m, 1 H), 7.47 - 7.52 (m, 3 H), 7.41 - 7.47 (m, 6 H), 7.38 - 7.40 (m, 4 H), 7.37 (d, *J*=1.83 Hz, 1 H), 7.31 (s, 1 H), 7.28 - 7.30 (m, 2 H), 7.25 - 7.26 (m, 1 H), 2.55 - 2.60 (s, 4 H), 1.73 (s, 4 H), 1.59 (s, 2 H), 1.46 (s, 18 H). ^{13}C NMR (125 MHz, $CDCl_3$) δ ppm 143.2, 140.8, 140.8, 139.7, 139.4, 139.3, 139.0, 138.6, 138.5, 131.0, 130.9, 130.2, 129.9, 126.2, 126.2, 125.8, 125.5, 125.2, 125.1, 124.7, 123.9, 123.8, 123.8, 123.6, 123.4, 123.4, 123.1, 120.3, 120.1, 120.1, 118.5, 118.4, 116.3, 109.7, 109.6, 109.5, 109.4, 109.1, 46.3, 38.3, 34.7, 32.0, 26.6, 23.2.

Synthesis of Cy-tmCPBN (9)

Compound **8** (300 mg, 0.32 mmol), compound **3** (295 mg, 0.39 mmol), K_2CO_3 (89 mg, 0.65 mmol), and $Pd(PPh_3)_4$ (18 mg, 0.01 mmol) were taken under a nitrogen atmosphere. Then, 30 mL of a degassed solvent mixture of toluene-methanol-water (2:1:1) was added. The reaction mixture was stirred under a nitrogen atmosphere at 120 °C for 6 h. After cooling to room temperature, the reaction mixture was filtered through a Celite pad. The resulting crude product was purified by silica gel column chromatography using CH_2Cl_2 and hexane (1:5) as the elution solvents. The purified product was filtered using methanol to obtain Cy-tmCPBN as a yellow solid (325 mg, 62% yield). ^{1}H NMR (500 MHz, $CDCl_3$) δ (ppm) 9.11 (d, *J* = 1.83 Hz, 2H), 8.54 (s, 2H), 8.45 (d, *J* = 1.53 Hz, 2H), 8.40 (d, *J* = 8.85 Hz, 2H), 8.24 (d, *J* = 2.14 Hz, 2H), 8.15 - 8.22 (m, 4H), 8.10 - 8.14 (m, 3H), 7.94 (d, *J* = 7.93 Hz, 1H), 7.76 - 7.81 (m, 2H), 7.74 (t, *J* = 8.09 Hz, 1H), 7.68 - 7.71 (m, 1H), 7.66 (d, *J* = 7.93 Hz, 1H), 7.56 - 7.65 (m, 5H), 7.41 - 7.50

(m, 9H), 7.37 (t, J = 1.22, 7.78 Hz, 1H), 7.29 - 7.33 (m, 1H), 7.22 - 7.24 (m, 1H), 2.60 (s, 4H), 1.75 (s, 4H), 1.65 - 1.68 (m, 18H), 1.60 (s, 2H), 1.49 - 1.52 (m, 18H), 1.43 (s, 18H). ^{13}C NMR (125 MHz, $CDCl_3$) δ ppm 145.4, 145.1, 144.8, 144.7, 143.7, 143.2, 141.7, 141.0, 140.8, 139.7, 139.4, 138.9, 138.7, 138.6, 138.5, 138.3, 130.9, 130.6, 129.8, 127.1, 126.5, 126.2, 126.1, 125.8, 125.1, 125.1, 124.6, 123.9, 123.7, 123.7, 123.5, 123.4, 120.7, 120.3, 120.0, 120.0, 118.5, 117.3, 116.3, 114.2, 109.9, 109.7, 109.6, 109.1, 107.0, 84.3, 77.2, 38.3, 35.2, 34.8, 34.7, 32.2, 32.0, 31.8, 26.6, 23.2. MALDI-TOF: m/z 1482.8 [M]. Elemental Anal. Calcd for $C_{108}H_{104}BN_5$: C, 87.48; H, 7.07; N, 4.72. Found: C, 87.33; H, 7.22; N, 4.69.

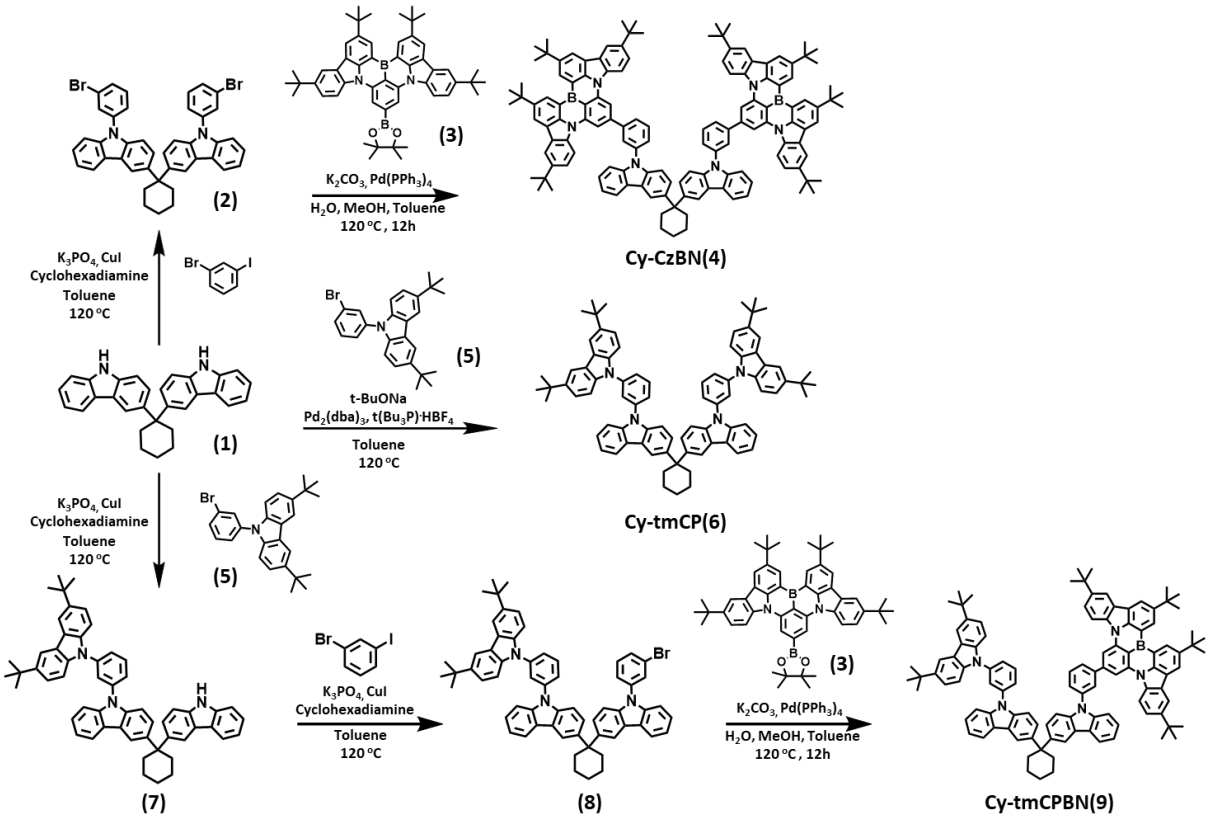

Scheme S1. Synthetic procedure for Cy-tmCP, Cy-CzBN, and Cy-tmCPBN.

3. NMR Spectra

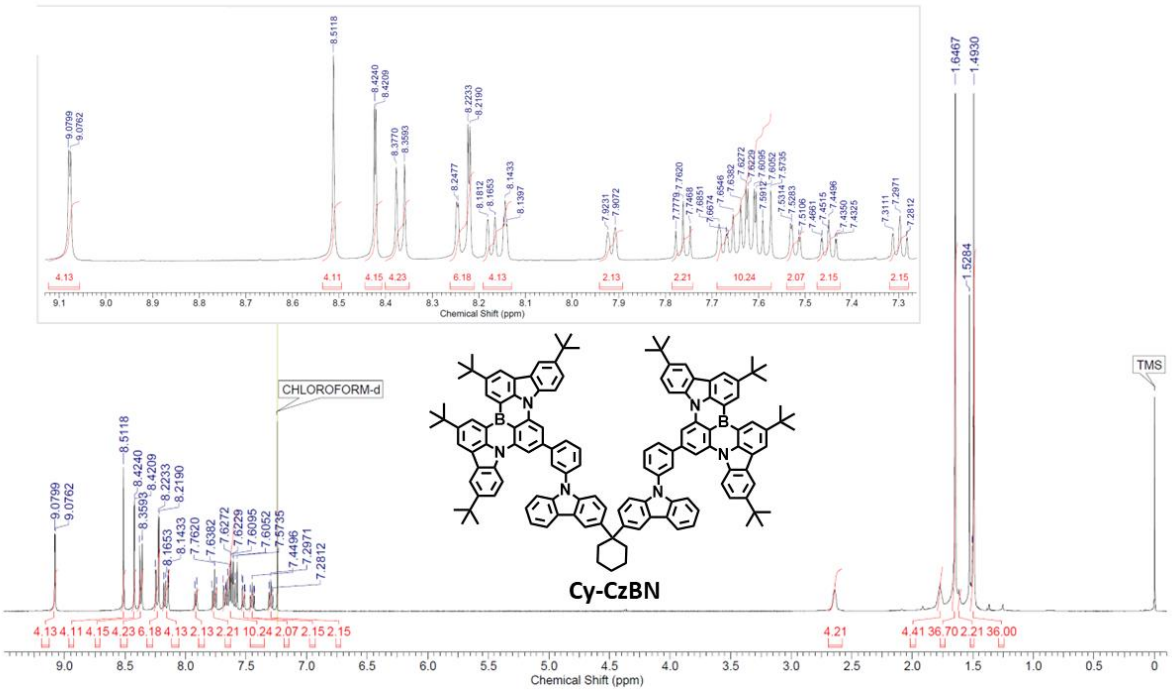

Fig. S1. ^{1}H NMR spectrum of Cy-CzBN.

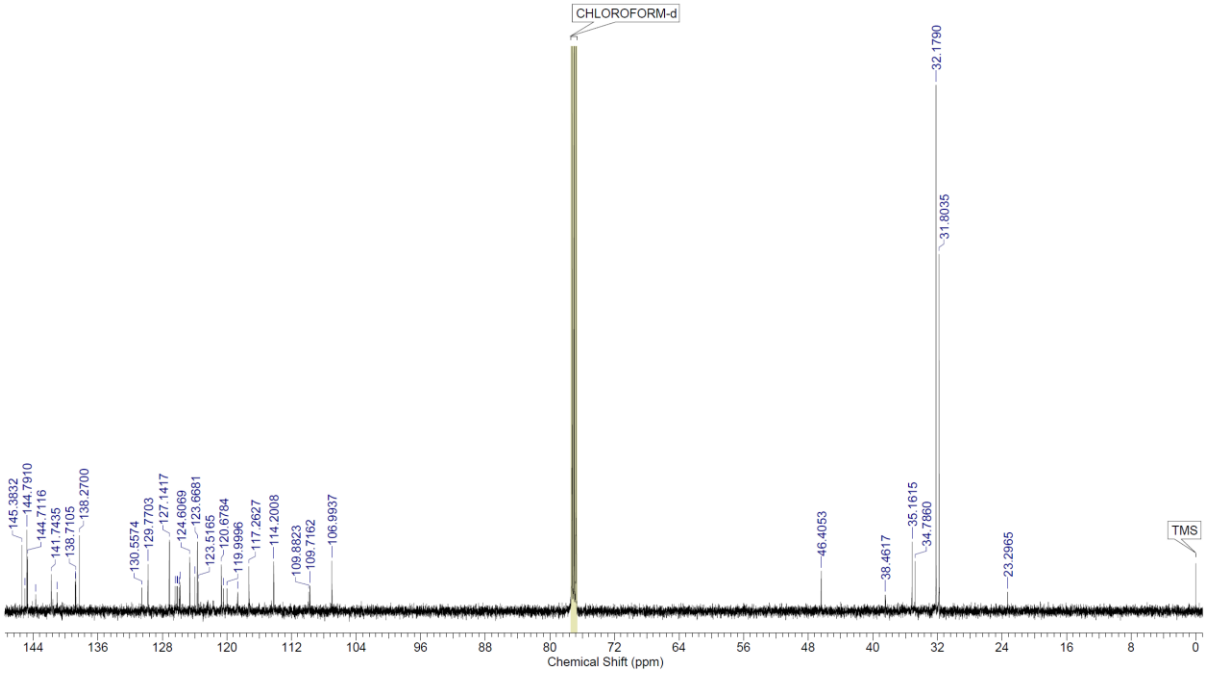

Fig. S2. ^{13}C NMR spectrum of Cy-CzBN.

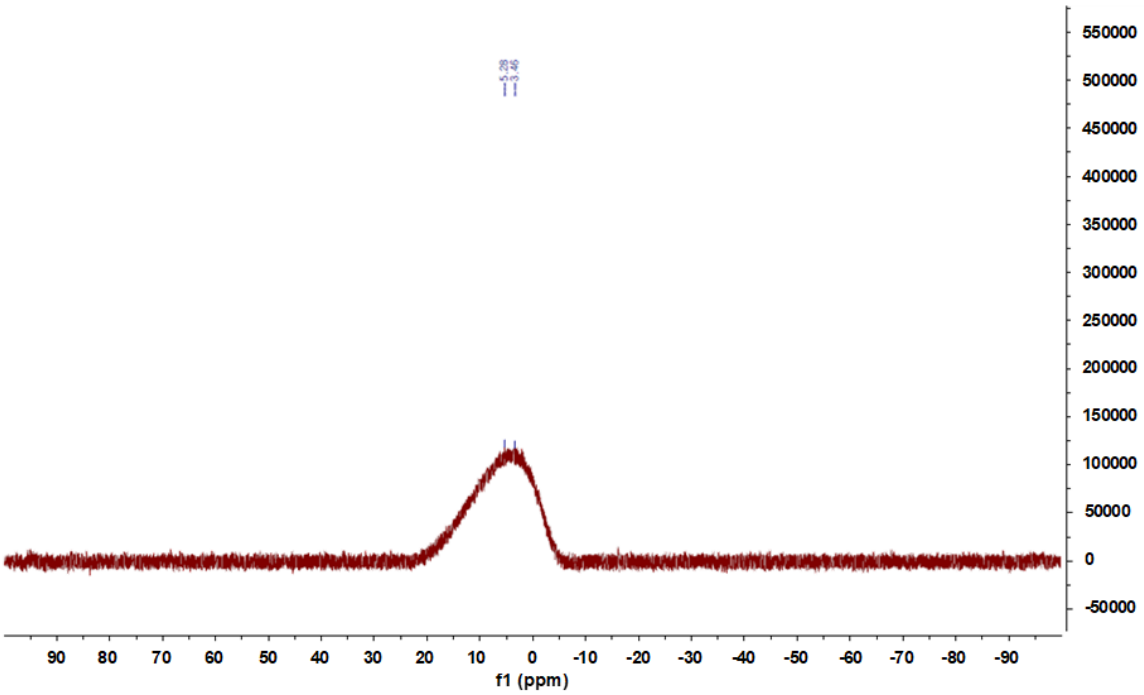

Fig. S3 ^{11}B NMR spectrum of Cy-CzBN.

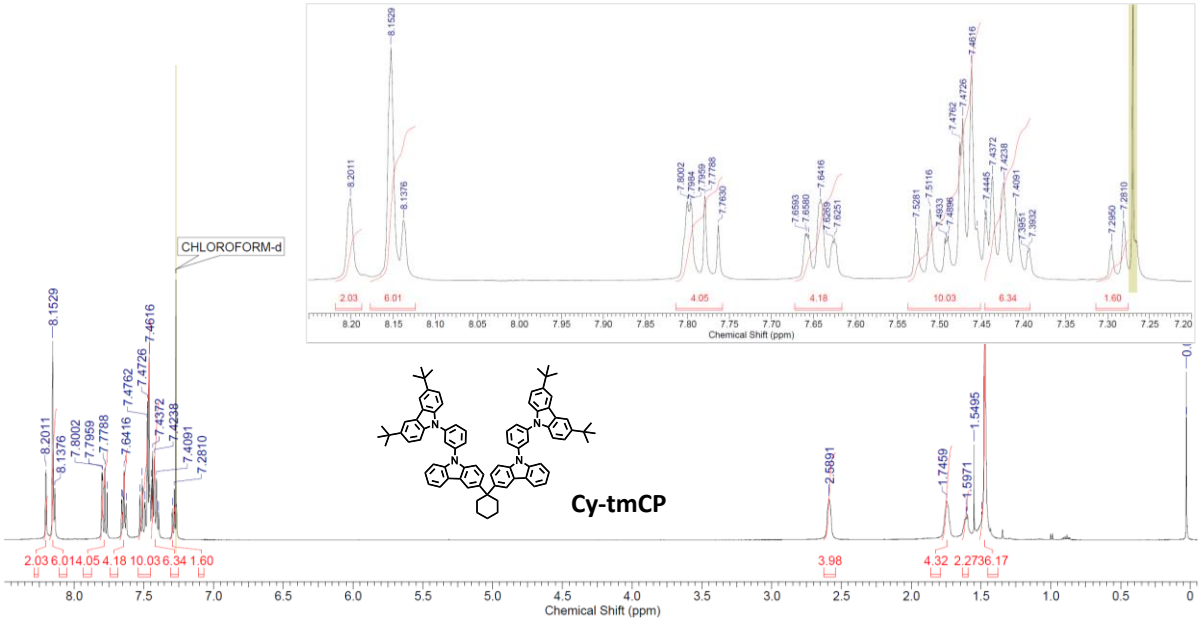

Fig. S4. ^{1}H NMR spectrum of Cy-tmCP.

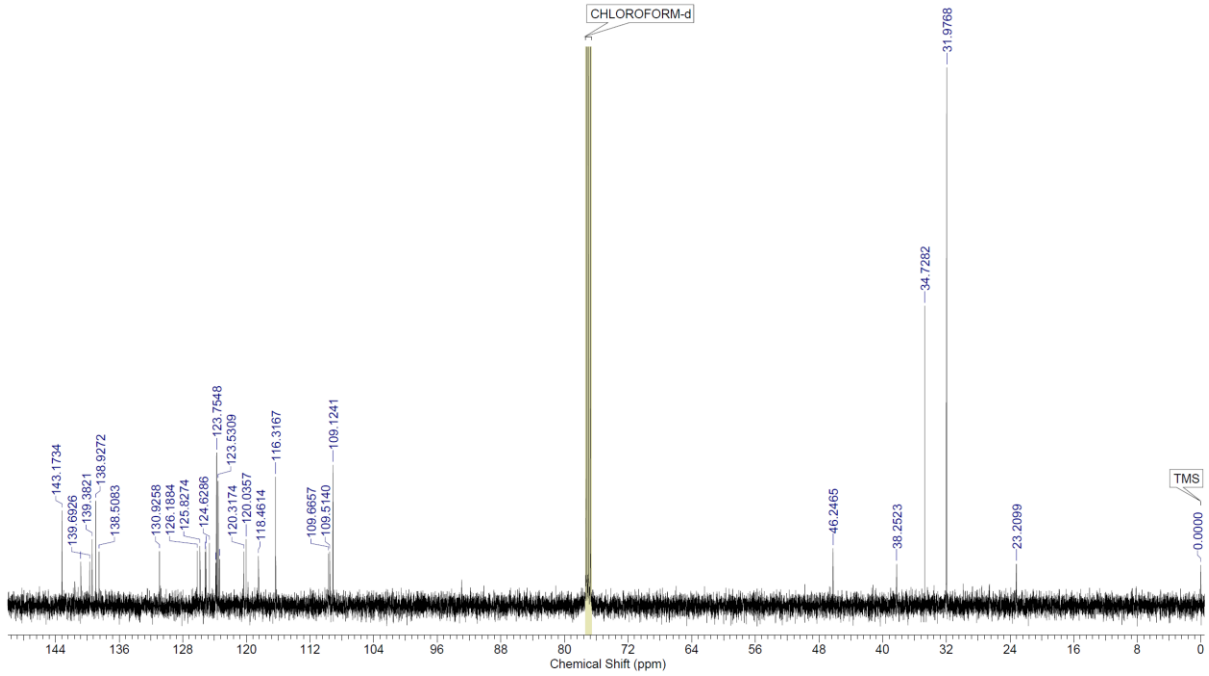

Fig. S5. ^{13}C NMR spectrum of Cy-tmCP.

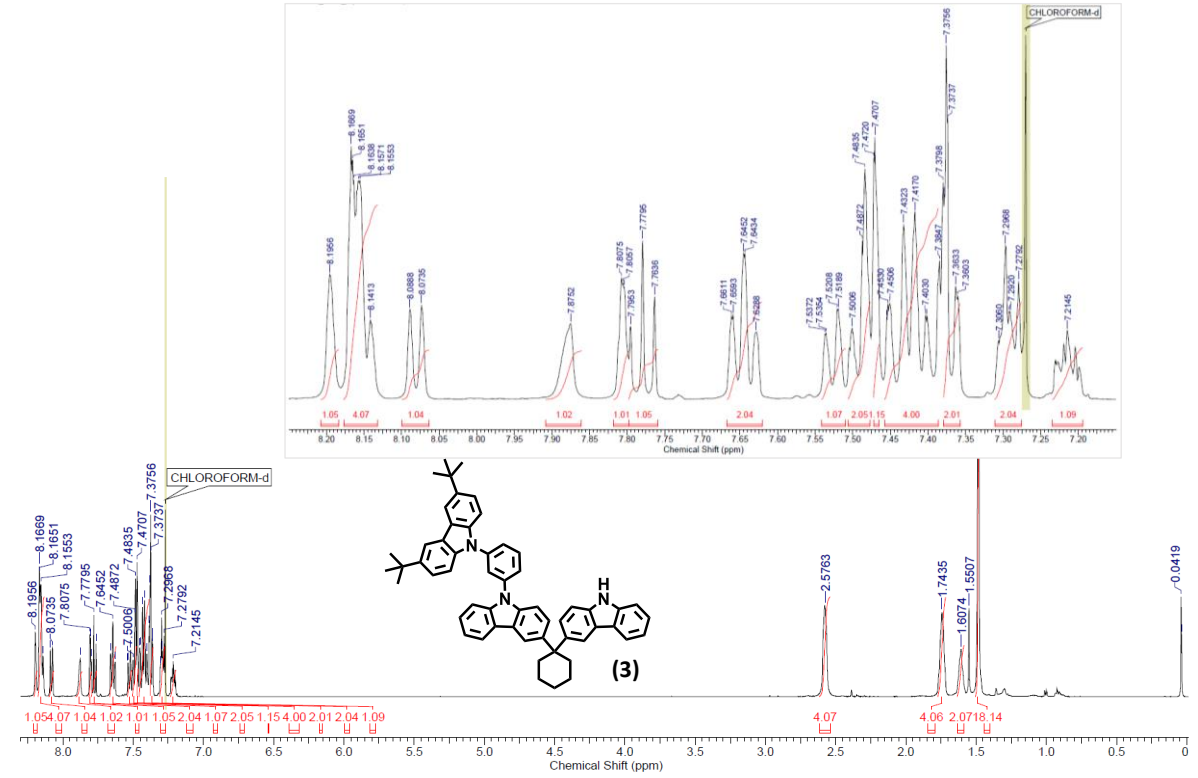

Fig. S6. ^{1}H NMR spectrum of *9-(3-(3-(1-(9H-carbazol-3-yl)cyclohexyl)-9H-carbazol-9-yl)phenyl)-3,6-di-tert-butyl-9H-carbazole (7)*.

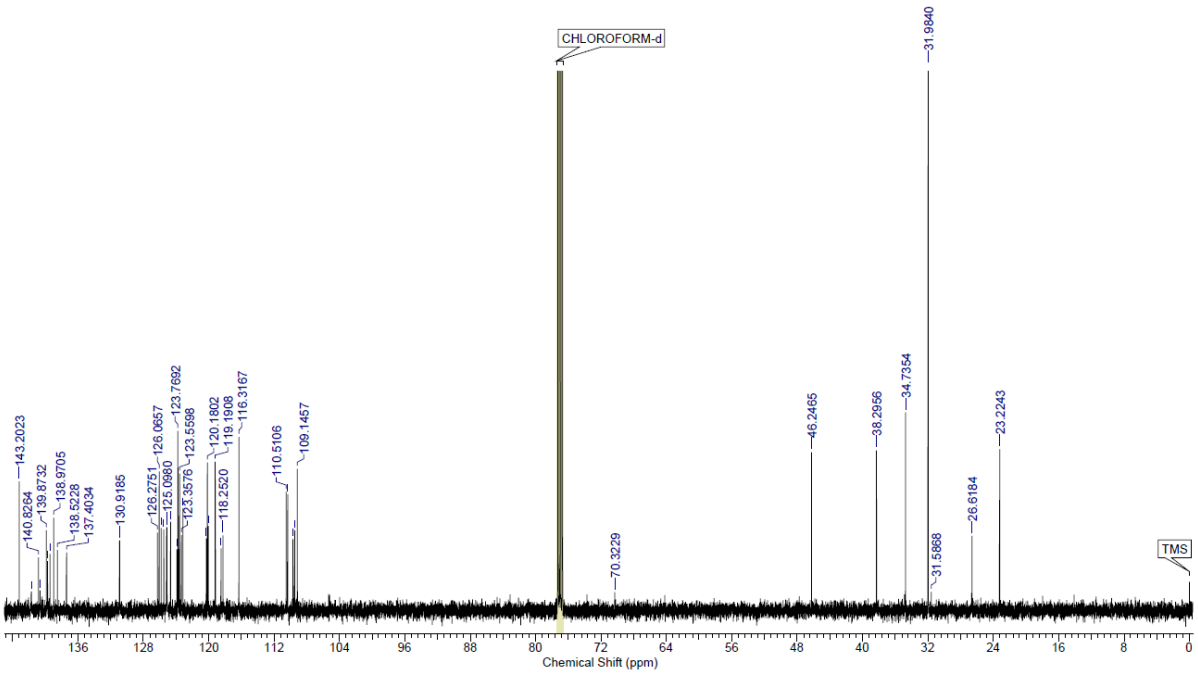

Fig. S7. ^{13}C NMR spectrum of *9-(3-(3-(1-(9H-carbazol-3-yl)cyclohexyl)-9H-carbazol-9-yl)phenyl)-3,6-di-tert-butyl-9H-carbazole (7)*.

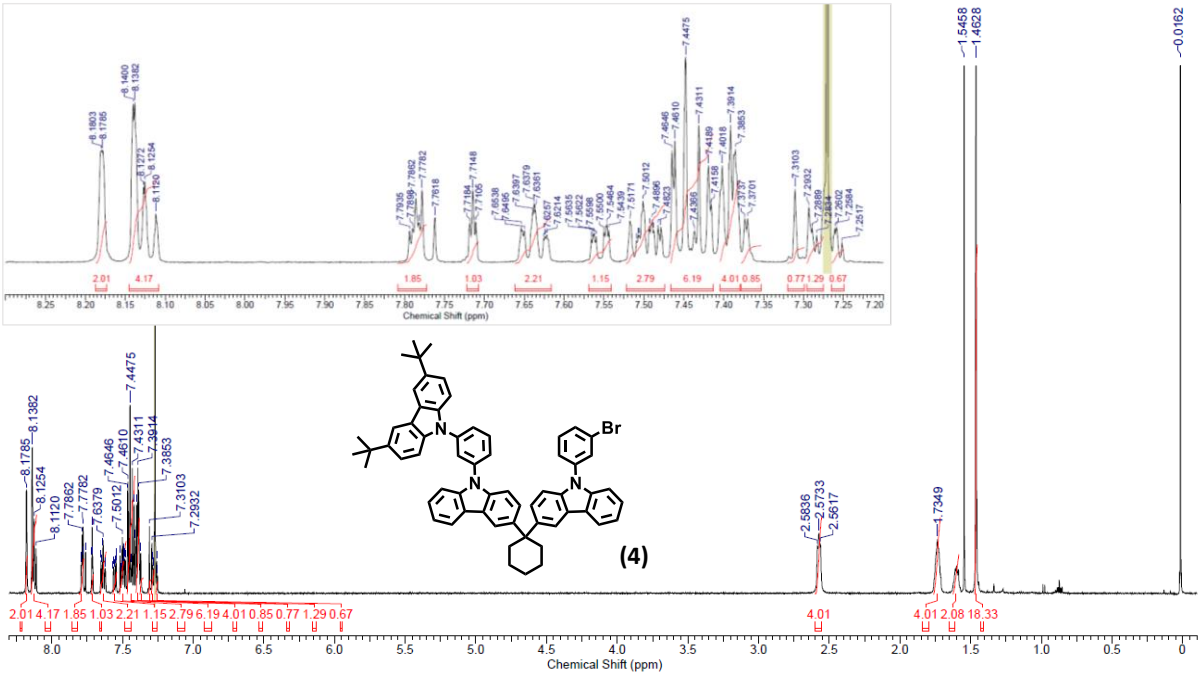

Fig. S8. ^{1}H NMR spectrum of *9-(3-(3-(1-(9-(3-bromophenyl)-9H-carbazol-3-yl)cyclohexyl)-9H-carbazol-9-yl)phenyl)-3,6-di-tert-butyl-9H-carbazole (8)*.

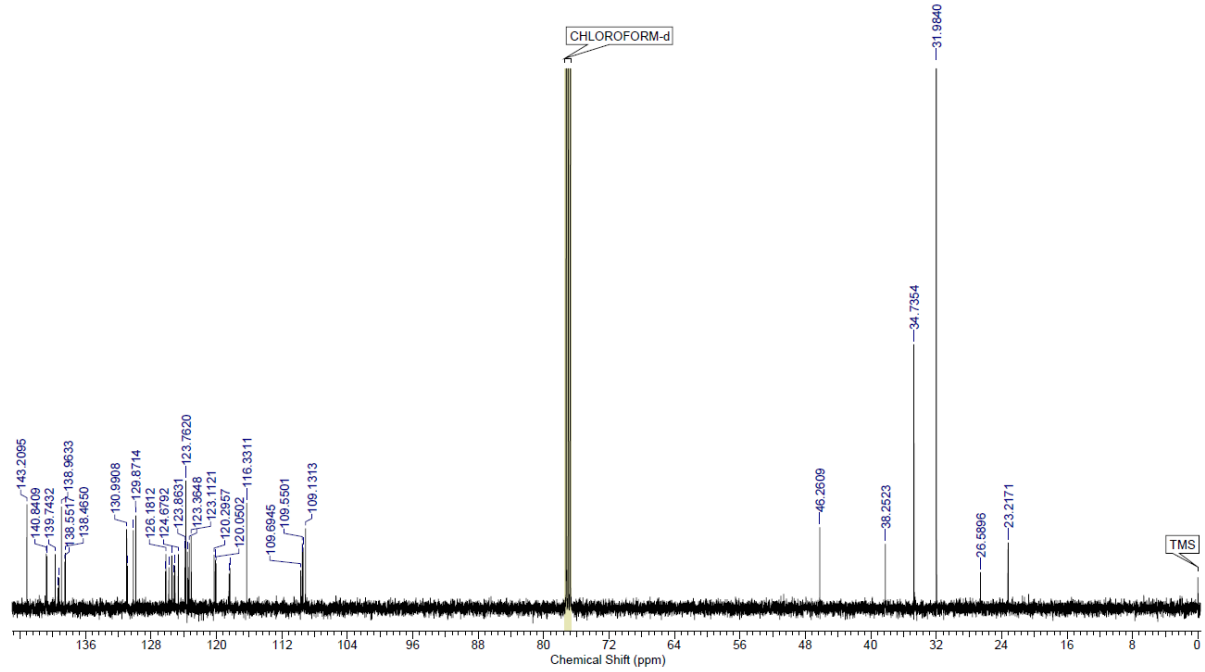

Fig. S9. ^{13}C NMR spectrum of *9-(3-(3-(1-(9-(3-bromophenyl)-9H-carbazol-3-yl)cyclohexyl)-9H-carbazol-9-yl)phenyl)-3,6-di-tert-butyl-9H-carbazole (8)*.

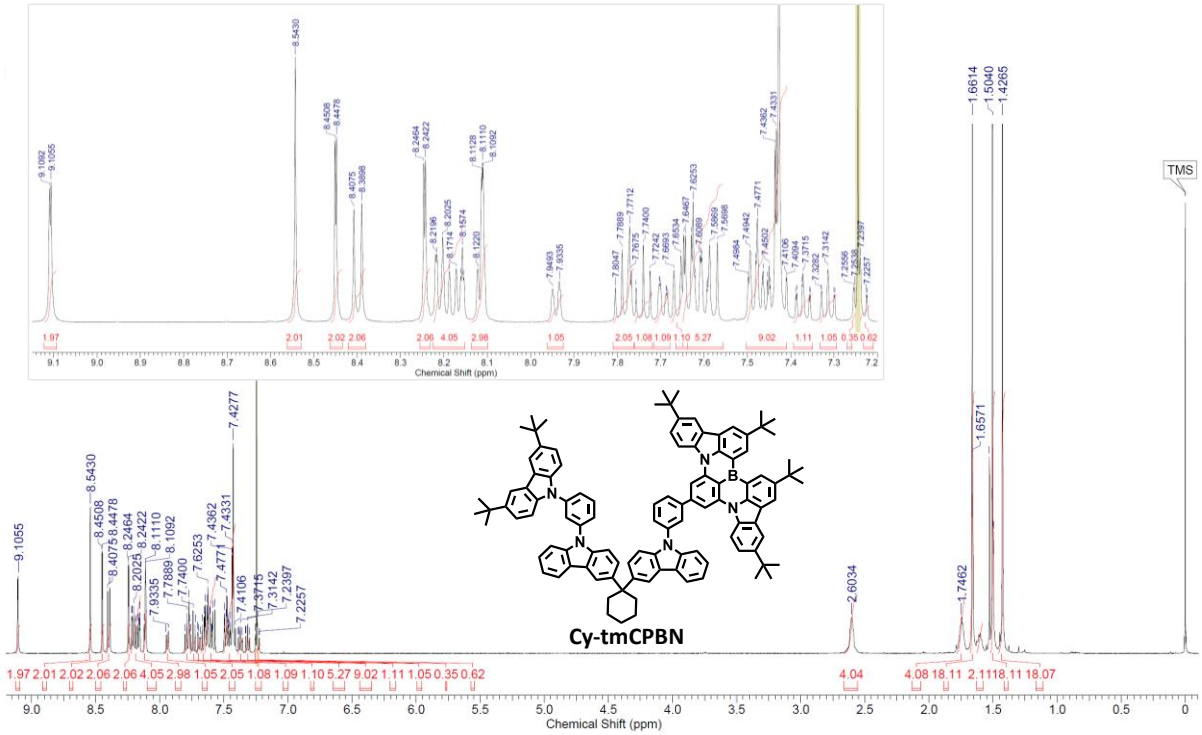

Fig. S10. ^{1}H NMR spectrum of Cy-tmCPBN.

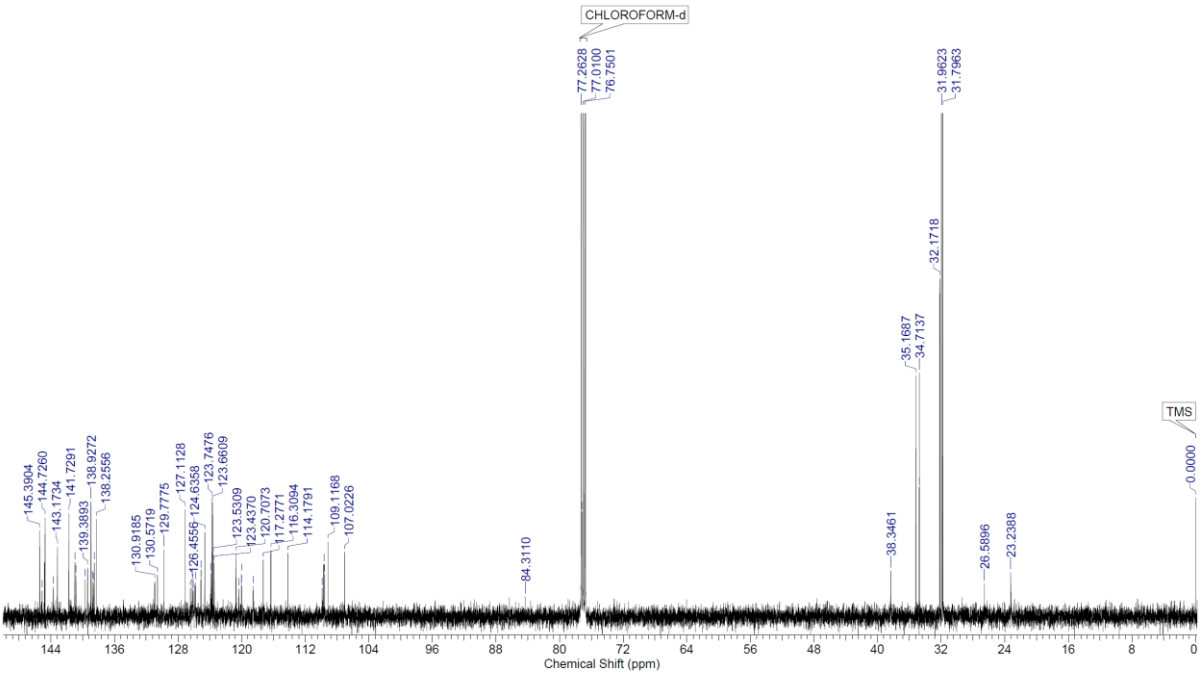

Fig. S11. ^{13}C NMR spectrum of Cy-tmCPBN

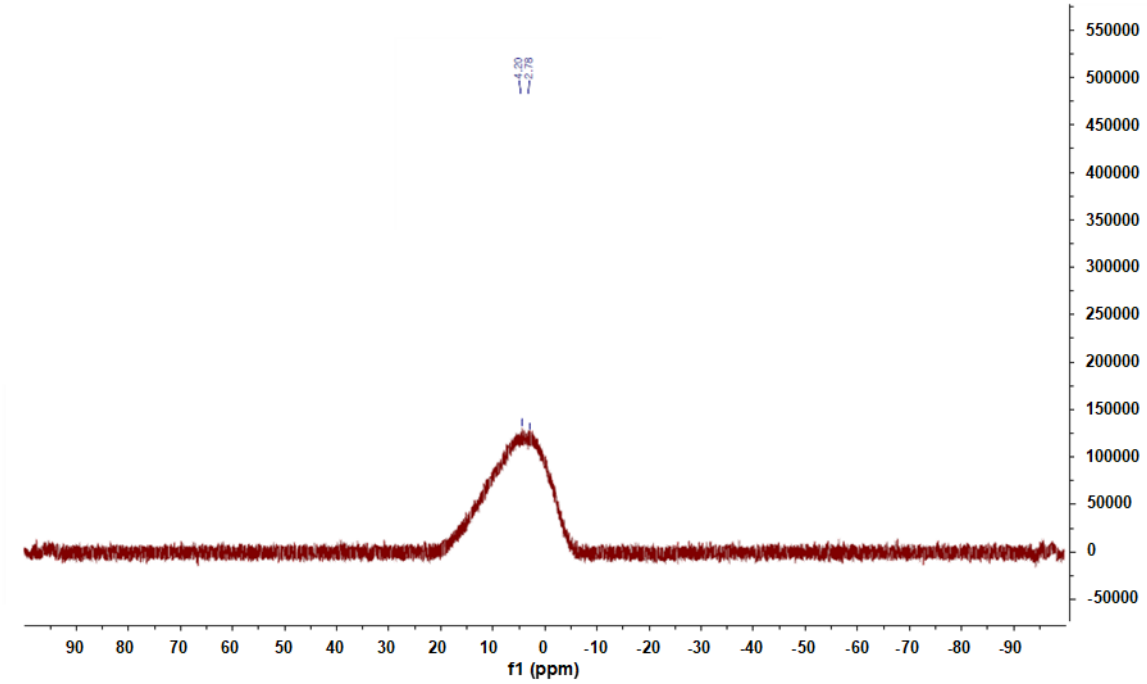

Fig. S12 ^{11}B NMR spectrum of Cy-tmCPBN.

4. Chemical Structure and MALDI-TOP Spectra

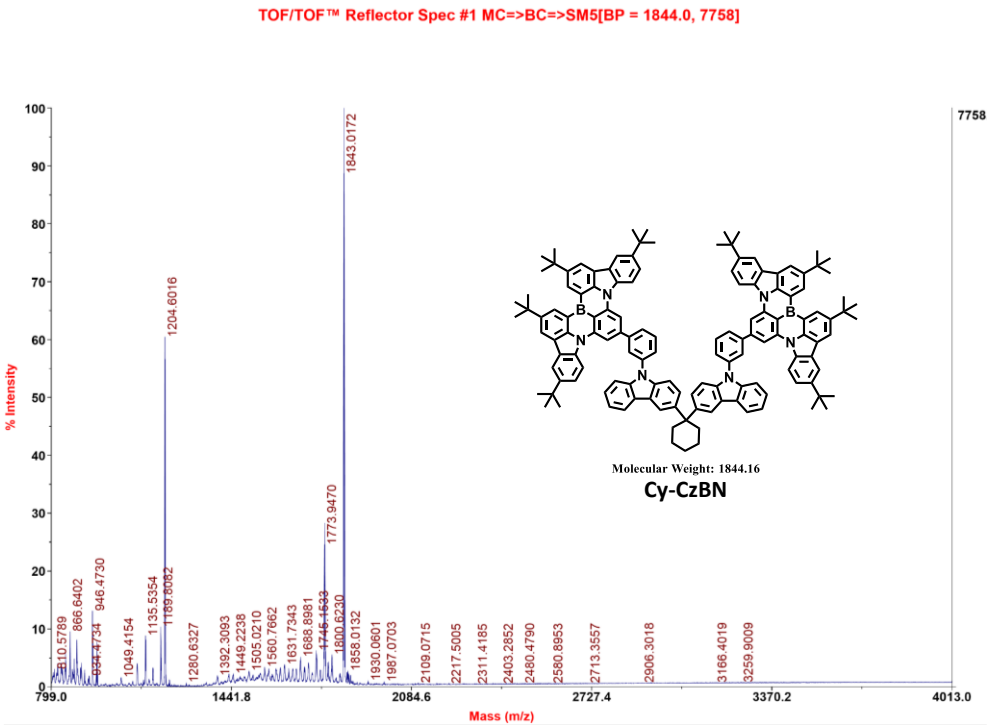

Fig. S13. MALDI-TOF spectrum of Cy-CzBN.

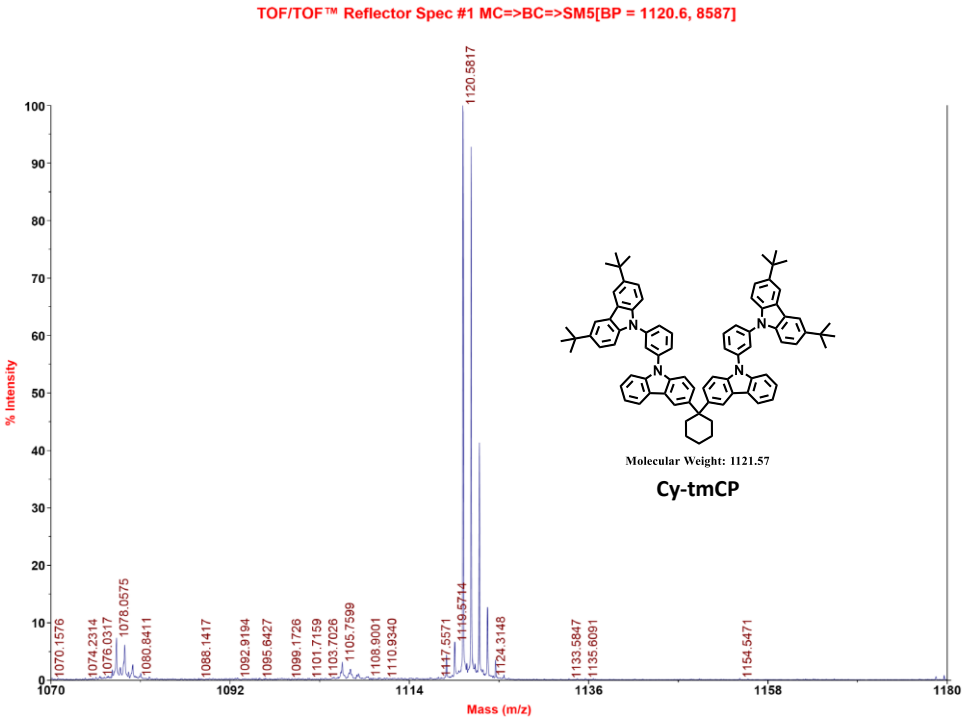

Fig. S14. MALDI-TOF spectrum of Cy-tmCP.

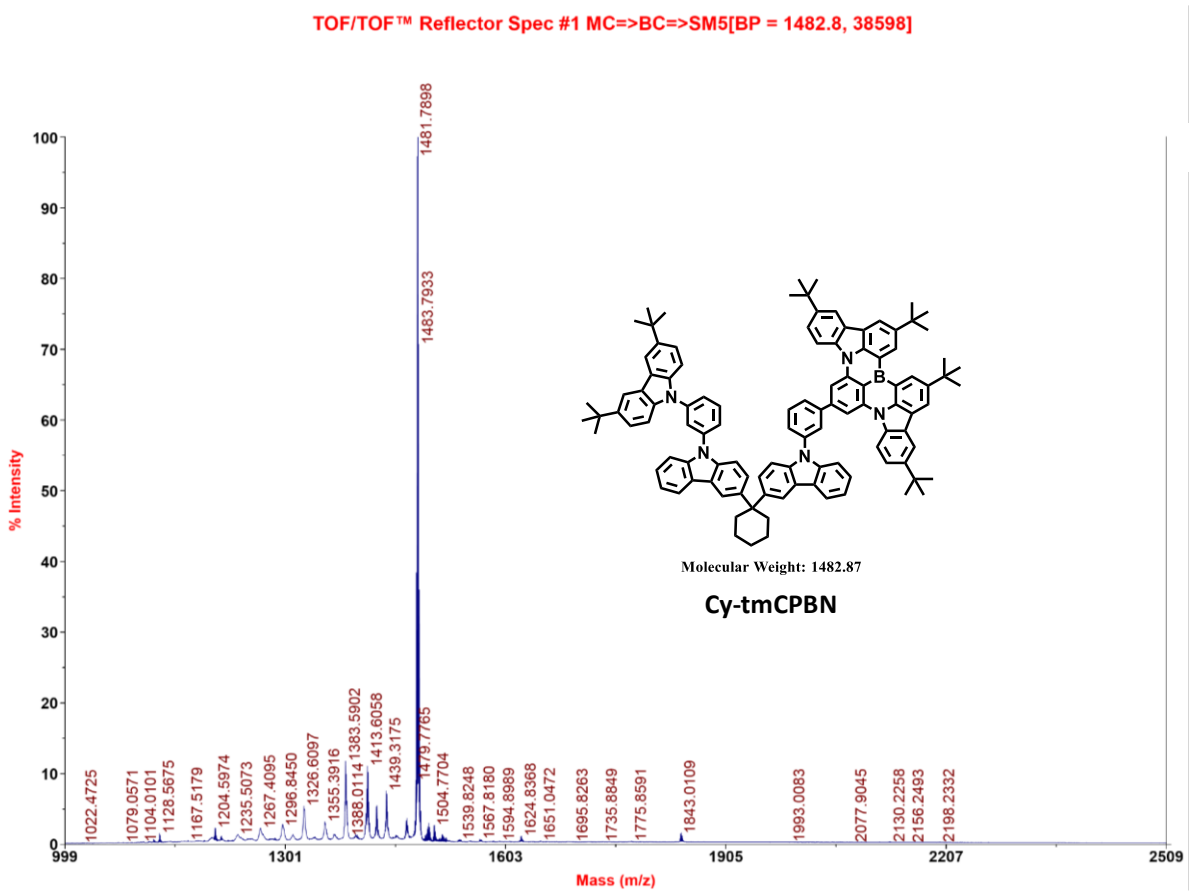

Fig. S15. MALDI-TOF spectrum of Cy-tmCPBN.

5. DFT Calculations

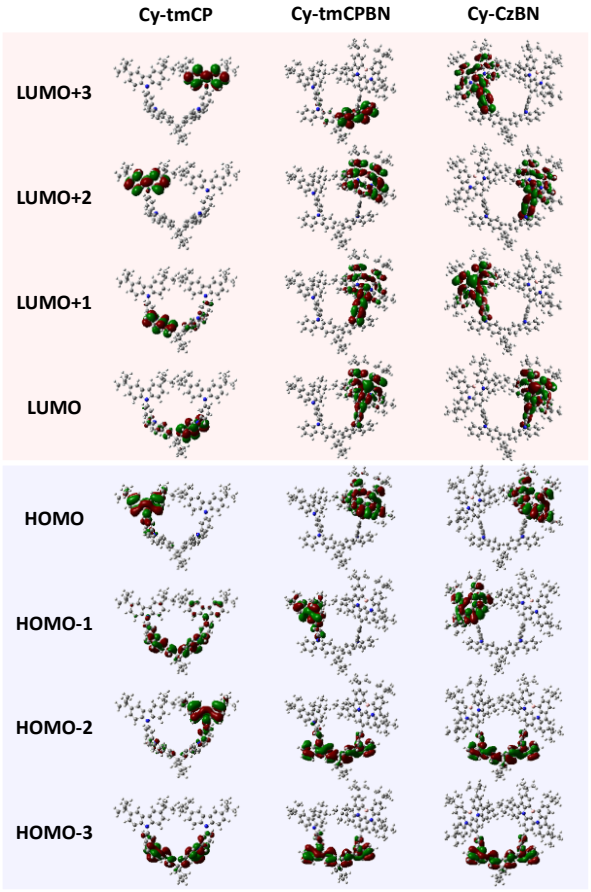

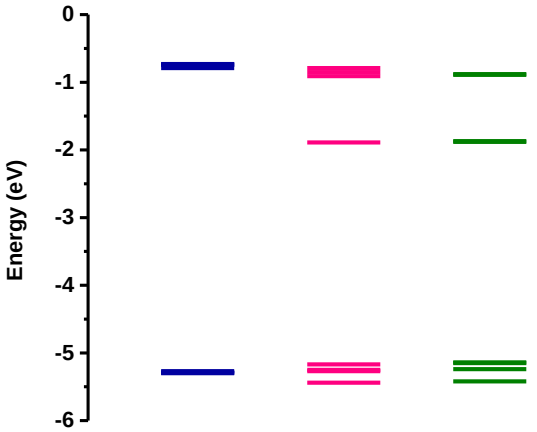

Energy Level (eV)	Cy-tmCP	Cy-tmCPBN	Cy-CzBN
LUMO+3	-0.73	-0.79	-0.88
LUMO+2	-0.74	-0.85	-0.89
LUMO+1	-0.74	-0.91	-1.87
LUMO	-0.79	-1.89	-1.88
HOMO	-5.27	-5.17	-5.14
HOMO-1	-5.29	-5.25	-5.15
HOMO-2	-5.29	-5.27	-5.24
HOMO-3	-5.30	-5.44	-5.42

Fig. S16. Optimized molecular structures, molecular orbitals and their energies of Cy-tmCP, Cy-tmCPBN, and Cy-CzBN obtained using the DFT calculations (B3LYP/6-31G(d)).

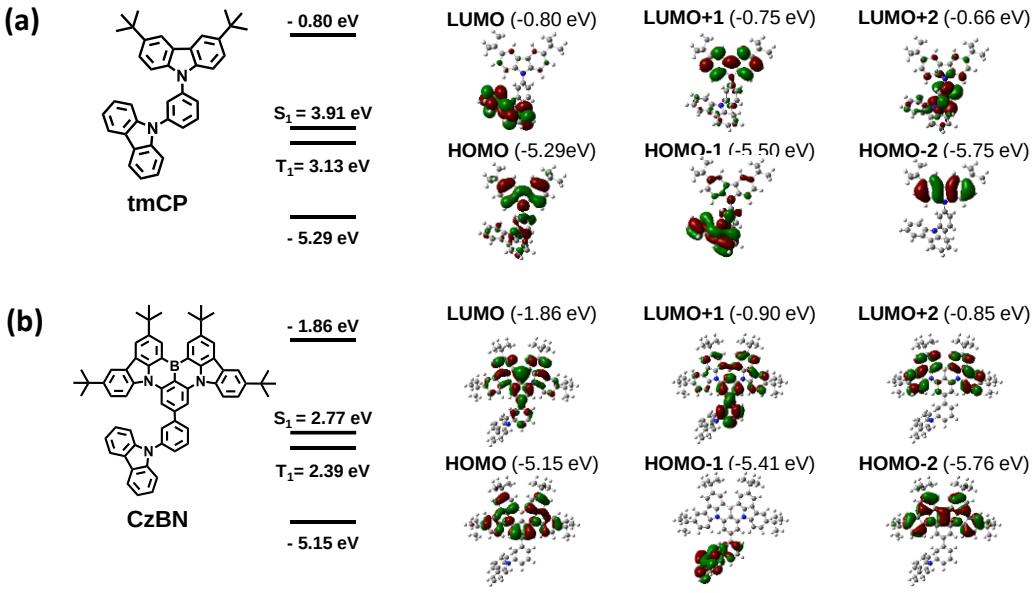

Fig. S17. Molecular orbitals and their energies of (a) tmCP and (b) CzBN units obtained using the DFT calculations (B3LYP/6-31G(d)).

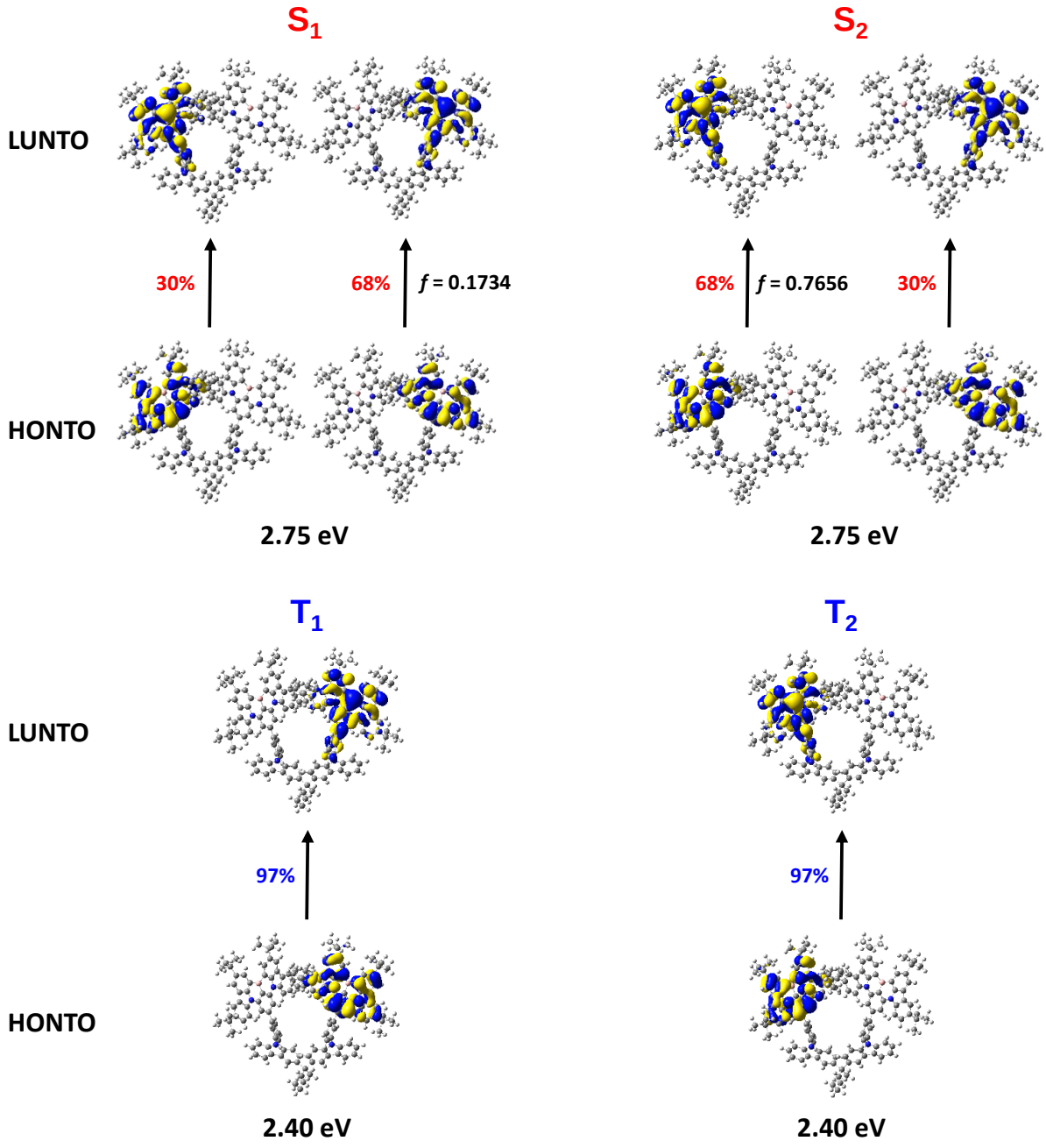

Fig. S18. Calculated natural transition orbitals (HONTO and LUNTO) of S_1, S_2, T_1, and T_2 for Cy-CzBN obtained using the DFT calculations.

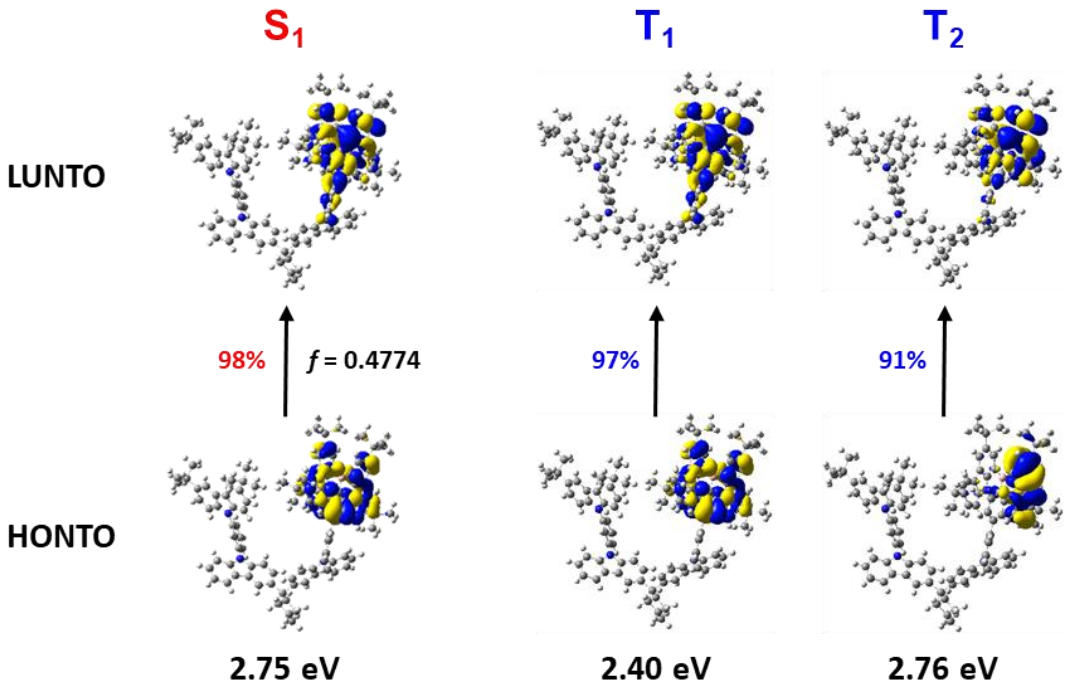

Fig. S19. Calculated natural transition orbitals (HONTO and LUNTO) of S_1, T_1, and T_2 for Cy-tmCPBN obtained using the DFT calculations.

6. Fundamental and Photophysical Properties

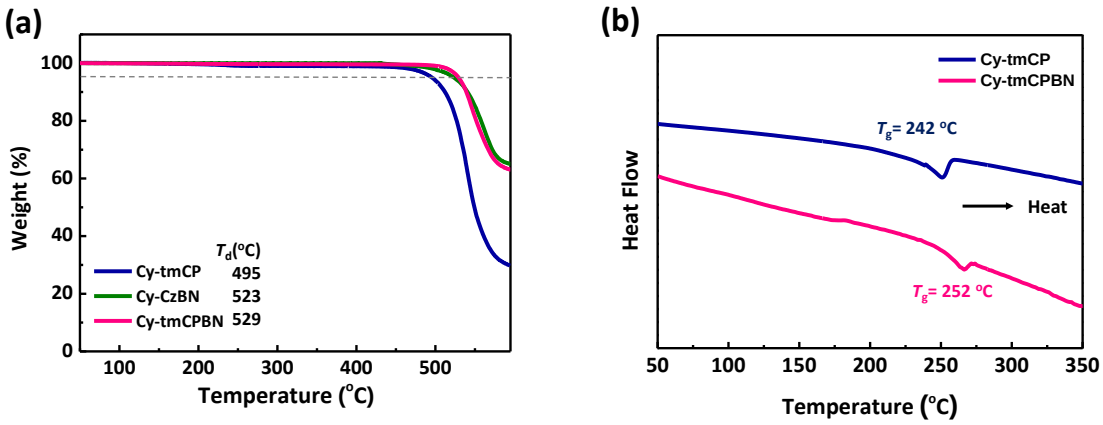

Fig. S20. (a) TGA thermograms, and (b) DSC traces of molecular dyads recorded at a heating rate of 10 °C/min under nitrogen atmosphere.

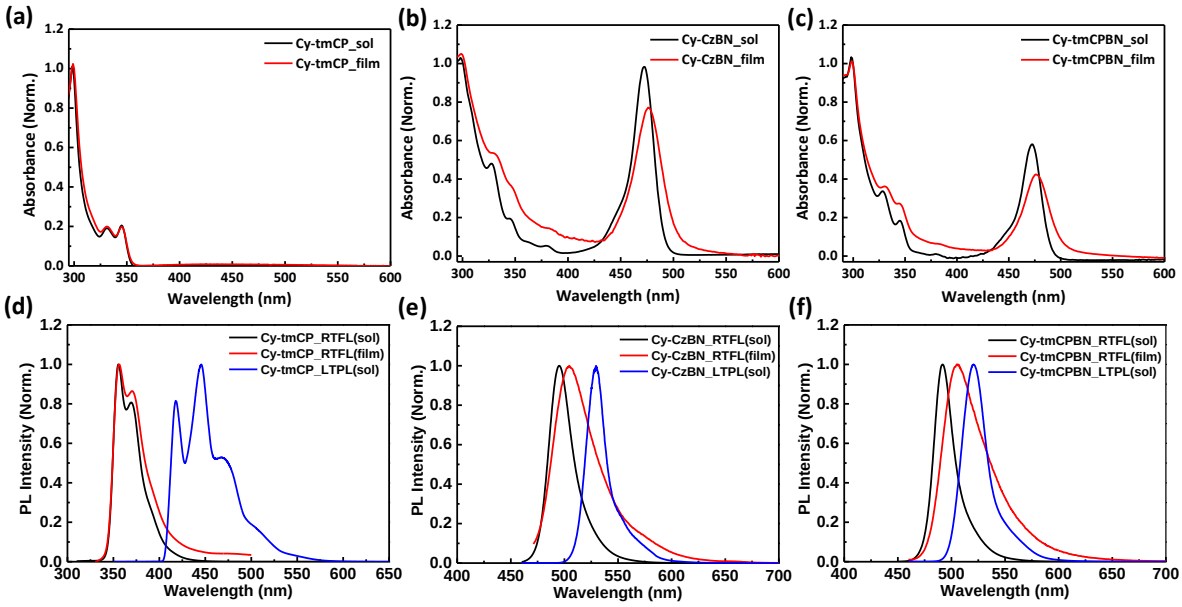

Fig. S21. (a-c) UV–vis absorption (Abs) and (d-f) fluorescence (FL), phosphorescence (Phos) spectra measured in toluene (1×10^{-5} M) and films.

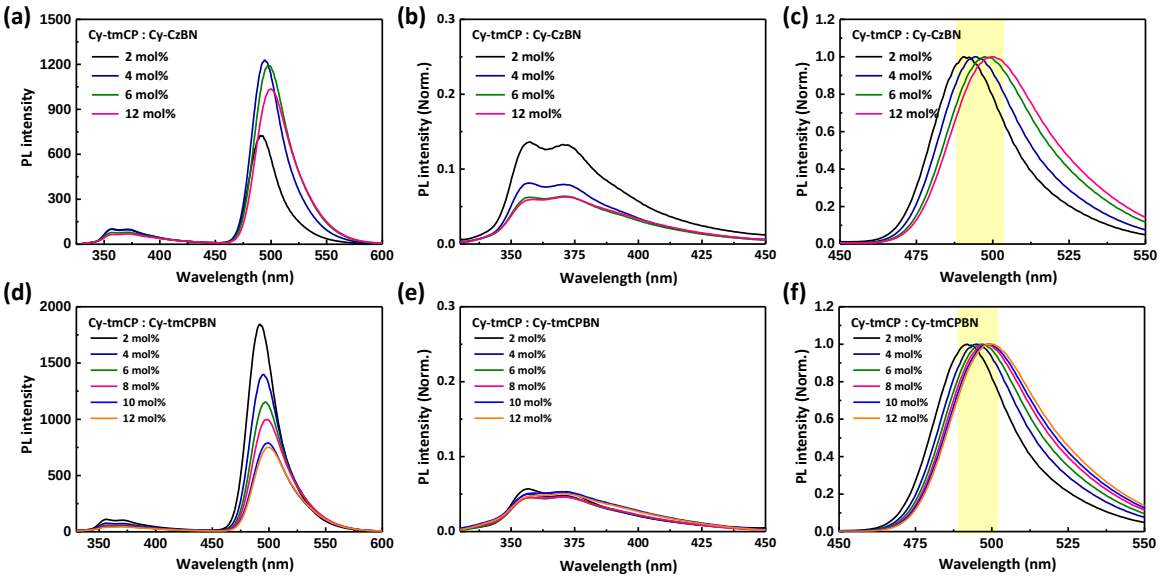

Fig. S22. PL spectra of doped films with varying emitter concentrations: (a-c) Cy-Cz BN emitters and (d-f) Cy-tmCPBN emitters.

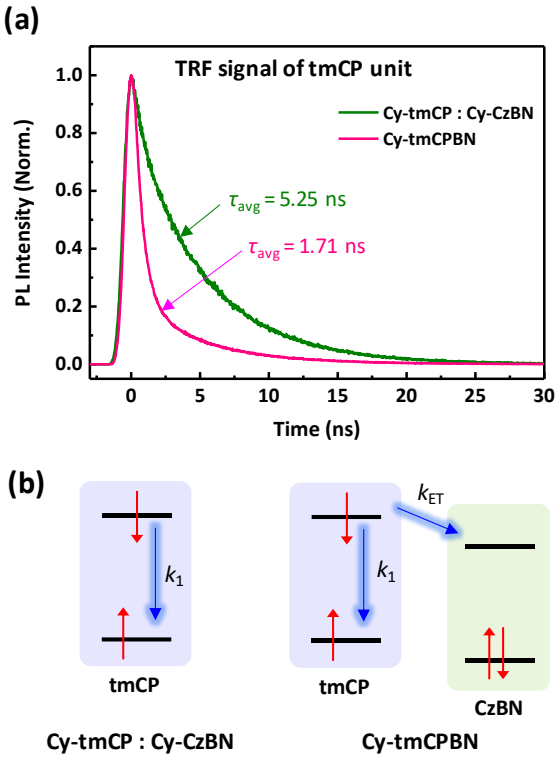

(c)

$$S(t) = a_1\exp(-t/\tau_1) + a_2\exp(-t/\tau_2)$$

$$\tau_{avg} = \frac{a_1\tau_1 + a_2\tau_2}{a_1 + a_2}$$

$$\tau_{avg} = \frac{1}{k_1 + k_{ET}} = 1.71 \text{ ns}$$

$$\tau_{avg} = \frac{1}{k_1} = 5.25 \text{ ns}$$

$$k_1 = 1.9 \times 10^8 \text{ s}^{-1}$$

$$k_{ET} = 3.9 \times 10^8 \text{ s}^{-1}$$

Fig. S23. (a) Time-resolved fluorescence signals measured with blend (Cy-tmCP:Cy-CzBN=1:1 mol%) and Cy-tmCPBN diluted toluene solution (~10^{-7} M) at 300 K (λ_{ex} = 340 nm). (b) Kinetic models illustrating the transfer mechanisms in the blend and Cy-tmCPBN. (c) TRF signal was analyzed by a bi-exponential function, and the average time constants was obtained. The energy transfer rate constant (k_{ET}) in Cy-tmCPBN was determined.

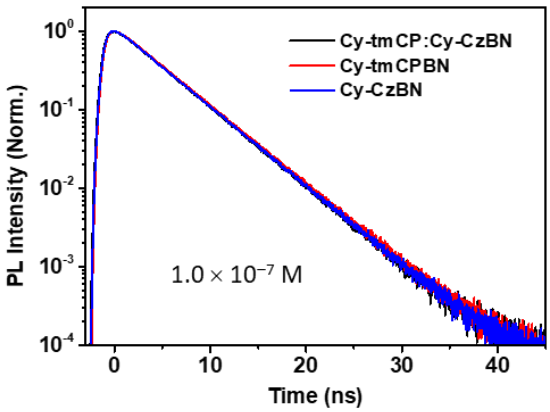

Fig. S24. Time-resolved fluorescence signals of CzBN units in diluted toluene solutions were measured at 488 nm (λ_{ex} = 340 nm). The TRF signals of CzBN units in two solutions are almost identical.

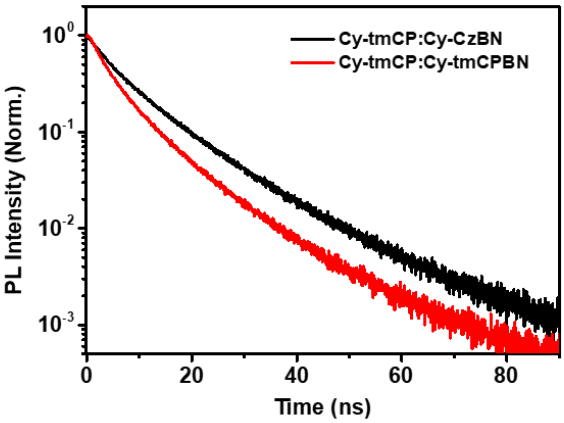

Fig. S25. Time-resolved fluorescence (TRF) signals of two doped films were measured at 488 nm (λ_{ex} = 340 nm). TRF signal of Cy-tmCPBN-doped Cy-tmCP films is faster than that of Cy-CzBN-doped Cy-tmCP films

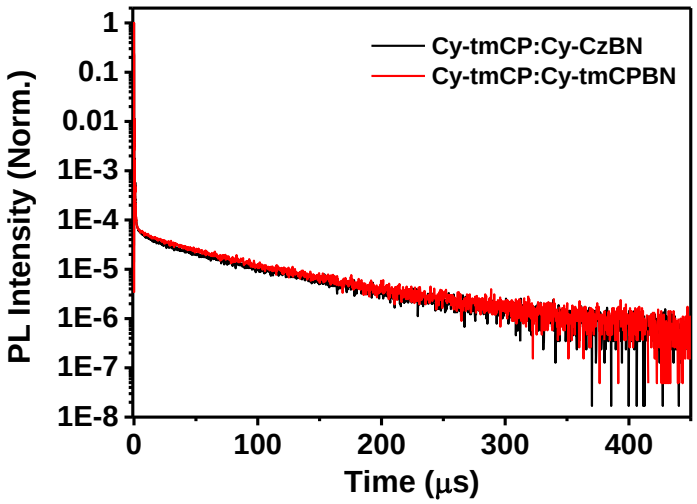

Fig. S26. TRPL signals of doped films with Cy-tmCP: Cy-CzBN and Cy-tmCP:Cy-tmCPBN.

Table S1. Quantum yields, lifetimes, and rate constants of 4 mol% doped Cy-CzBN and Cy-tmCPBN films in Cy-tmCP

Materials	Φ_{PL} (%)	Φ_p (%)	Φ_d (%)	τ_p (ns)	τ_d (μs)	$k_{r,S}$ ($\times 10^7$ s^{-1})	k_{ISC} ($\times 10^7$ s^{-1})	k_{RISC} ($\times 10^4$ s^{-1})	$k_{nr,S}$ ($\times 10^7$ s^{-1})	k_{ISC}/k_{RISC}
Cy-CzBN	42.3	34.6	7.7	10.7	78.8	3.2	1.7	1.6	4.4	1094.3
Cy-tmCPBN	54.5	42.7	11.8	10.1	80.2	4.2	2.1	1.6	3.5	1345.1

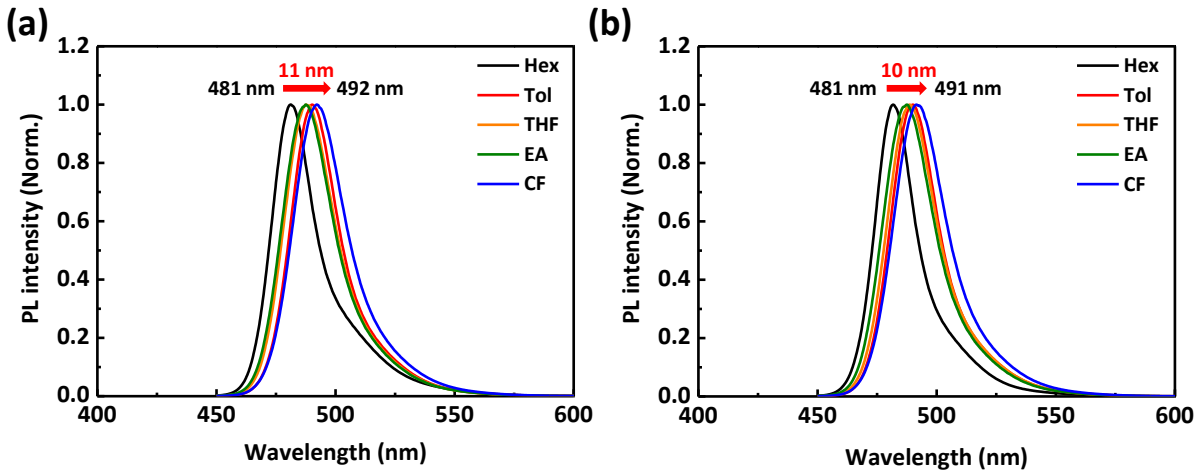

Fig. S27. Normalized PL spectra of (a) Cy-CzBN and (b) Cy-tmCPBN in different polarity solvents. [S5]

Table S2. The emission profiles of Cy-CzBN and Cy-tmCPBN in different solvents.

Solvent	**Solvent polarity [E_T(30)] (kcal mol^{-1})**	Cy-CzBN		Cy-tmCPBN	
		λ_{PL} (nm)	**FWHM (nm)**	**λ_{PL} (nm)**	**FWHM (nm)**
Hexane	31.0	481	20	481	21
Toluene	33.9	490	24	490	23
Tetrahydrofuran	37.4	487	26	488	25
Ethyl acetate	38.1	487	26	488	26
Chloroform	39.1	492	26	491	26

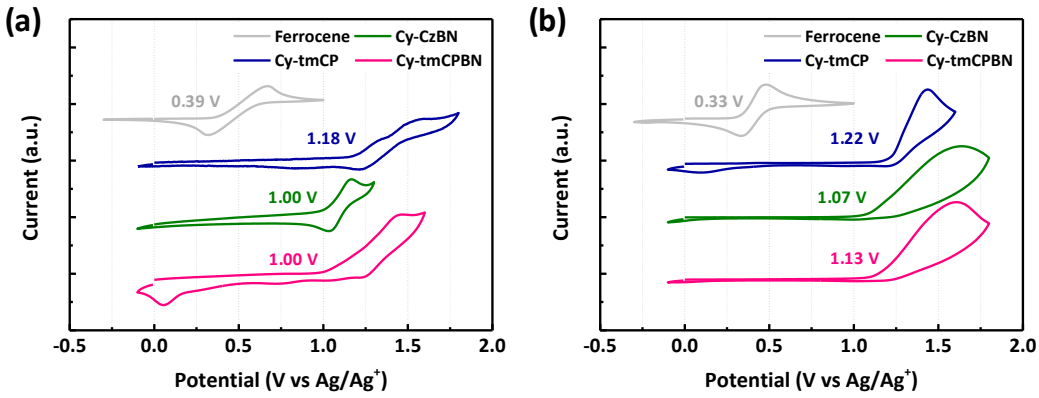

Fig. S28. Cyclic voltammograms of molecular dyads in (a) solution and (b) film state.

Table S3. Optical, photophysical and electrochemical properties of molecular dyads.

Compound	Absorption (nm)		PL (nm)		FWHM[a] (nm)	E_S/E_T[g] (eV)	E_g[c] (eV)	Energy level (eV)	
	Solution[a]	Film[b]	Solution[a]	Film[b]				HOMO[e]	LUMO[f]
Cy-tmCP	298, 345	299, 331, 345	355	355	30	3.61/3.06	3.50	-5.69	-2.19
Cy-CzBN	299, 473	299, 478	494	504	22	2.61/2.43	2.46	-5.54	-3.08
Cy-tmCPBN	297, 472	298, 476	491	505	22	2.62/2.50	2.47	-5.60	-3.13

[a] Measured in toluene solution. [b] Measured in the thin film state. [c] $1240/\lambda_{cut\text{-}off}$. [d] First oxidation onset points were obtained from cyclic voltammograms (sample: film on Pt electrode). [e] HOMO (eV) = -e(4.8 eV + E_{ox} - $E_{Ferrocene}$). [f] LUMO (eV) = HOMO (eV) + E_g (eV). [g] E_S and E_T energies were obtained from the onset of the fluorescence and phosphorescence spectra in toluene solution at 298K and 77K, respectively.

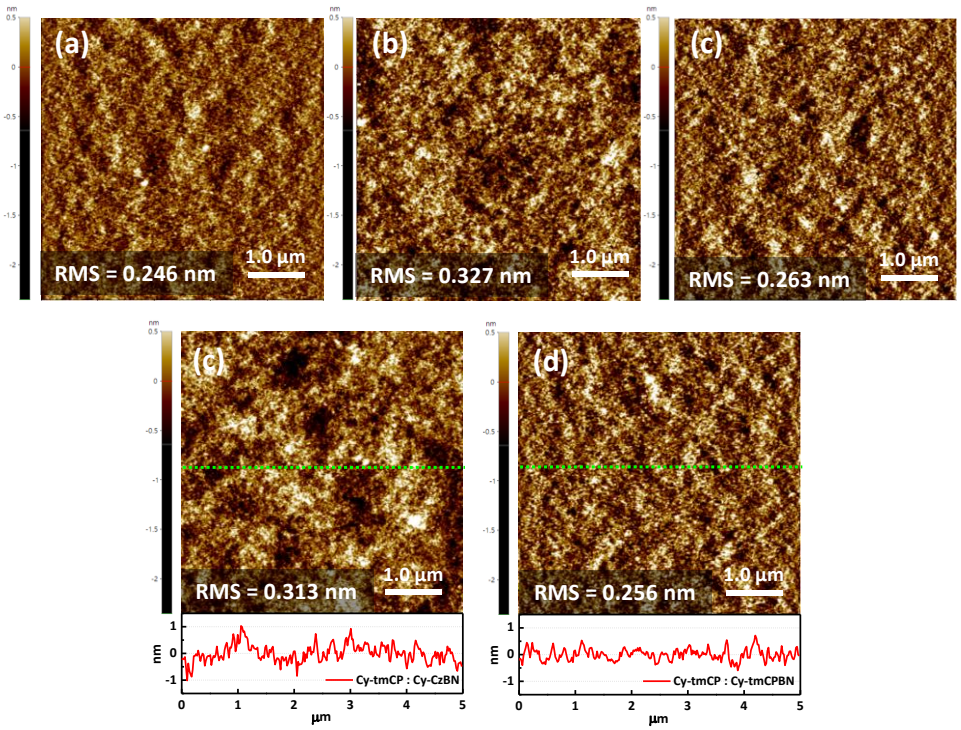

Fig. S29. (a-c) AFM height images of V-shaped molecule films : (a) Cy-tmCP, (b) Cy-CzBN, and (c) Cy-tmCPBN. (5μm × 5μm)

7. The Performance of MR-TADF OLED

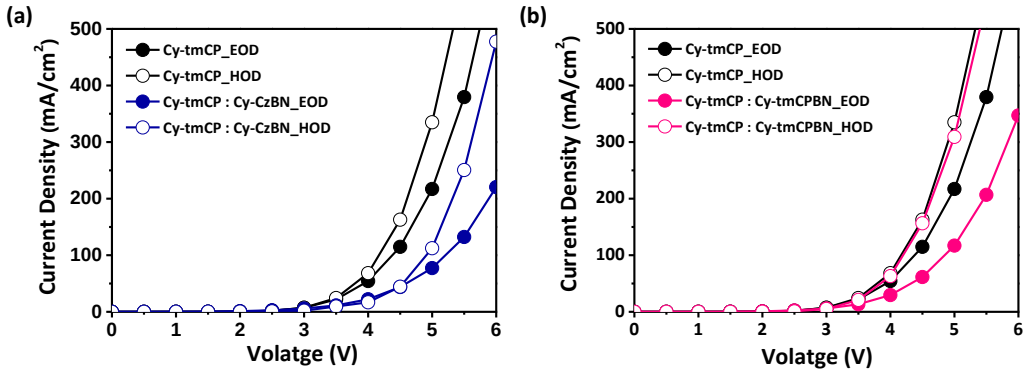

Fig. S30. *J-V* characteristics of HOD and EOD with (a) Cy-tmCP and Cy-CzBN doped films, (b) Cy-tmCP and Cy-tmCPBN doped films.

To investigate the charge balance in the emitting layers of OLEDs using two different emitters, hole-only devices (HOD) and electron-only devices (EOD) were fabricated. The HOD and EOD were constructed using the following structures: ITO/PEDOT:PSS (30 nm)/PX2Cz (20 nm)/EML (20 nm)/Al (100 nm) and ITO/Al (50 nm)/EML (20 nm)/BmPYPB (50 nm)/LiF (1 nm)/Al (100 nm). The current density–electric field (*J–V*) curves for all the devices are shown in **Fig. S30**.

For the Cy-tmCP film, the hole current density was relatively high under the same voltage because of the hole-affine nature of mCP, while maintaining a favorable balance between electrons and holes. For a film doped with Cy-CzBN in the host Cy-tmCP, the balance between the hole and electron currents remained largely unchanged. Nevertheless, the addition of the dopant led to a decrease in both current densities, which was attributed to a reduction in the carrier mobility between the mCP units. However, in the case of the Cy-tmCP film doped with Cy-tmCPBN, the hole current density in the HOD was similar to that of Cy-tmCP, as the hole transport ability was dominated by the tmCP moiety. Compared to the Cy-CzBN blend film, the Cy-tmCPBN blend film showed a slightly larger difference in hole and electron currents under the same voltage, but demonstrated a significantly higher overall current. This result suggests that the intramolecular energy transfer observed in Cy-tmCPBN leads to improved current density, implying that the dual-functional molecular dyad strategy can be an effective method for developing advanced emitter materials for TADF-OLEDs. [S6,S7]

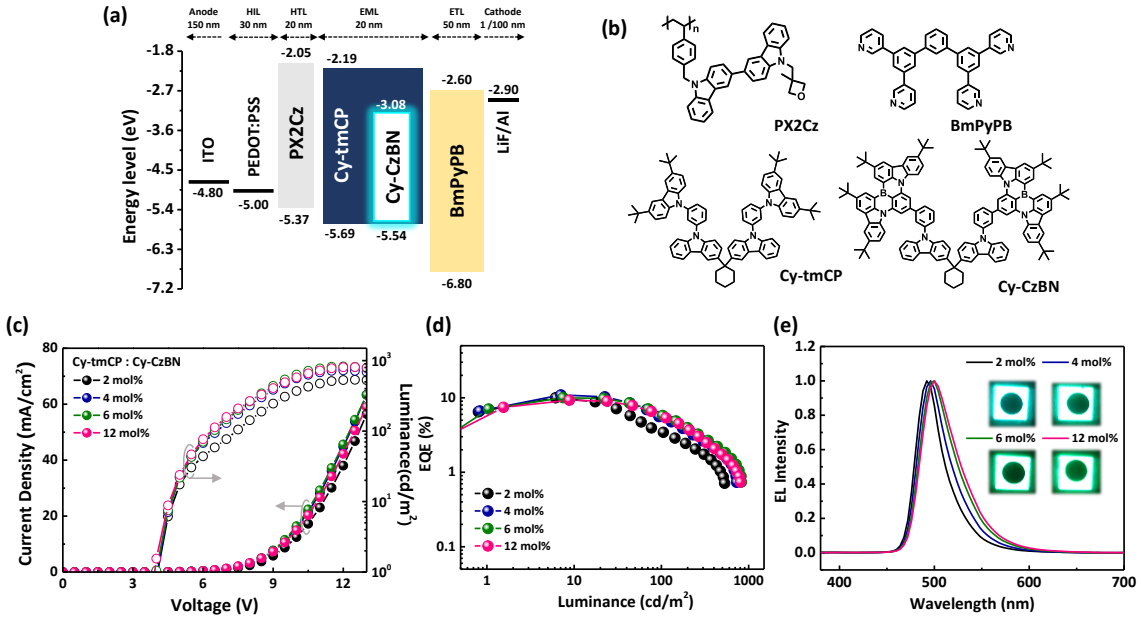

Fig. S31. (a) Device configurations and energy diagram of the solution-processed TADF-OLEDs. (b) Chemical structures of the materials employed in the devices. (c) Current density–voltage–luminance (*J*–*V*–*L*) curves and (d) external quantum efficiency (EQE) curves of the devices. (e) EL spectra of the Cy-tmCP films doped with x mol% Cy-CzBN.

Table S4. EL performance of the solution-processed TADF-OLEDs based on Cy-tmCP at Cy-CzBN.

Emitter	Doping conc.	V_{on} [a] (V)	$\eta_{c,max}$ [b] (cd/A)	$\eta_{p,max}$ [c] (lm/W)	L [d] (cd/m^2)	$\eta_{ext,max}$ [e] (%)	λ_{EL} (nm)	FWHM (nm)	CIE (x, y)
Cy-CzBN	2 mol%	4.01	22.03	15.38	535	9.99	492	33	(0.11,0.45)
	4 mol%	4.01	26.73	18.66	727	10.90	496	38	(0.12,0.52)
	6 mol%	3.95	26.81	18.71	827	10.03	500	43	(0.14,0.56)
	12 mol%	3.81	25.81	18.02	807	9.27	500	45	(0.15,0.58)

[a] Turn-on voltage at 1 cd/m^2. [b] Maximum current efficiency. [c] Maximum power efficiency. [d] Maximum luminance. [e] Maximum external quantum efficiency.

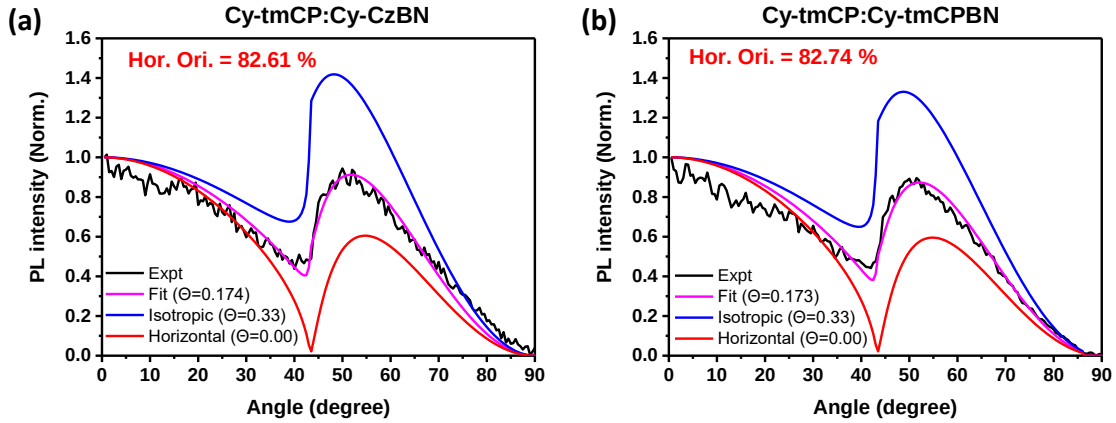

Film on Quartz	Cy-tmCP:Cy-CzBN	Cy-tmCP:Cy-tmCPBN
Thickness (nm)	20	20
n_{eff}	1.50	1.55
n_x	1.519	1.594
n_z	1.462	1.458
Θ	0.1739	0.1726
Vertical (%)	17.39	17.26
Horizontal (%)	82.61	82.74

Fig. S32. Angle-dependent PL intensities of p-polarized light at 355 nm from 20-nm-thick films composed of Cy-tmCP : Cy-CzBN and Cy-tmCP : Cy-tmCPBN.

Table S5. Summary of the device performance of highly-efficient solution-processed TADF-OLEDs and this work.

Emitter	λ_{PL}/FWHM(sol) [nm]	$S_1/T_1/\Delta E_{ST}$	EQE_{max}	λ_{EL}/FWHM [nm]	CIE(x,y)	REF
Cy-CzBN	**494/22**	**2.61/2.43/0.18**	**12.33**	**496/36**	**0.11,0.50**	**This work**
Cy-tmCPBN	**491/22**	**2.62/2.50/0.12**	**10.90**	**496/38**	**0.12,0.52**	
4FlCzBN	493/23	2.60/2.52/0.08	10.9	500/29	0.11.0.57	S8
DtCzBN	492/22	2.61/2.45/0.16	11.1	492/29	0.11,0.48	S9
Cy-DtCzBN	492/22	2.61/2.43/0.18	12.7	492/29	0.10,0.47	S9
PCzDBN2	423/22	2.63/2.57/0.06	17.9	479/28	0.11,0.25	S10
BON-D1	476/28	2.61/2.47/0.14	13.4	488/39	0.13,0.44	S11
BSeN-Cz	476/26	2.71/2.59/0.1	18.0	482/35	0.11,0.30	S12
BSeN-DCz	475/26	2.72/2.60/0.12	19.1	479/32	0.11,0.24	S12
BSeN-TCz	474/26	2.72/2.60/0.12	19.7	478/31	0.11,0.21	S12
ICz-TDBA	416/49	2.98/2.79/0.19	13.0	431/45	0.16,0.05	S13
PIdCz-TDBA	424/43	2.92/2.72/0.20	12.2	433/43	0.16,0.04	S13
5CzBN-12CSP	488/-	2.81/2.72/0.09	17.6	508/-	0.23,0.50	S14
phCz-2-5CzBN	509/-	2.86/2.79/0.07	18.8	496/29	0.16,0.49	S15

8. References

S1. S. Sem, S. Jenatsch, K. Stavrou, A. Danos, A. P. Monkman, B. Ruhstaller, *J. Mater. Chem. C,* 2022, **10**, 4878.

S2. N. Y. Kwon, S. H. Park, C. W. Koh, J. Y. Park, M. J. Kang, H. I. Baek, J. Youn, S. Park, C. W. Han, M. J. Cho, D. H. Choi, *ACS Appl. Mater. Interfaces*., 2023, **15**, 28277.

S3. Y. Xu, C. Li, Z. Li, J. Wang, J. Xue, Q. Wang, X. Cai, Y. Wang, *CCS Chem.,* 2022, **4**, 2065.

S4. D. Chercka, S. J. Yoo, M. Baumgarten, J. J. Kim, K. Müllen, *J. Mater. Chem. C,* 2014, **2**, 9083.

S5. C. Reichardt, *Chem. Rev.,* 1994, **94**, 2319.

S6. H. Xu, K. Yin, W. Huang, *Chem. Eur. J.* 2007, **13**, 1028.

S7. J. Y. Lee, *Appl. Phys. Lett.* 2006, ***89*****,** 223517.

S8. N. Peethani, N. Y. Kwon, C. W. Koh, S. H. Park, J. M. Ha, M. J. Cho, H. Y. Woo, S. Park, D. H. Choi, Adv. Opt. Mater., 2023, 12, 2301217.

S9. J. Y. Park, N. Y. Kwon, C. W. Koh, S. H. Park, M. J. Kang, H. Kwak, C. Y. Park, W. S. Chae, C. S. Hong, S. Park, M. J. Cho, D. H. Choi, ACS Appl. Mater. Interfaces., 2024, 16, 16553-16562.

S10. W. Luo, T. Wang, Z. Huang, H. Huang, N. Li, C. Yang, Adv. Funct. Mater., 2023, 34, 2310042.

S11. J. Liu, L. Chen, X. Wang, Q. Yang, L. Zhao, C. Tong, S. Wang, S. Shao, L. Wang, Macromol. Rapid Commun., 2022, 43, e2200079.

S12. L. Yang, P. Wang, K. Zhang, S. Wang, S. Shao, L. Wang, Dyes Pigm., 2023, 216, 111371.

S13. B. Chen, C. Liao, D. Li, H. Liu, S. Wang, *J. Mater. Chem. C,* **2023**, 11, 8767-8775.

S14. Z. Zhang, G. Zhao, H. Chen, T. Zhou, W. Tian, W. Jiang, *Org. Electron*., 2024, 128, 107043.

S15. G. Zhao, R. Zhou, G. Zhang, H. Chen, X. Wang, Z. Zhang, W. Tian, W. Jiang, *Adv. Opt. Mater,* **2023**, 11, 2203065.